AFCRL-64-292 March 1964

SCIENTIFIC REPORT NO. 1

TRANSVERSE FOCAL REGION OF A SPHERICAL REFLECTOR

Part 1: Geometric Optics

BY ROY C. SPENCER AND GEOFFREY HYDE

CONTRACT NO. AF 19(628)2758

PROJECT NO. 4600, TASK NO. 460007

RADIO CORPORATION OF AMERICA
MISSILE AND SURFACE RADAR DIVISION
MOORESTOWN, NEW JERSEY

PREPARED FOR

AIR FORCE CAMBRIDGE RESEARCH LABORATORIES
OFFICE OF AEROSPACE RESEARCH
UNITED STATES AIR FORCE
BEDFORD MASSACHUSETTS

AFCRL CONTRACT MONITOR: OTHO KERR

NOTICES

Requests for additional copies by Agencies of the Department of Defense, their contractors, and other government agencies should be directed to:

DEFENSE DOCUMENTATION CENTER (DDC)
CAMERON STATION
ALEXANDRIA, VIRGINIA 22314

Department of Defense contractors must be established for DDC services or have their 'need-to-know' certified by the cognizant military agency of their project or contract."

All other persons and organizations should apply to the:

U.S. DEPARTMENT OF COMMERCE
OFFICE OF TECHNICAL SERVICES
WASHINGTON 25, D. C.

DISCLAIMER NOTICE

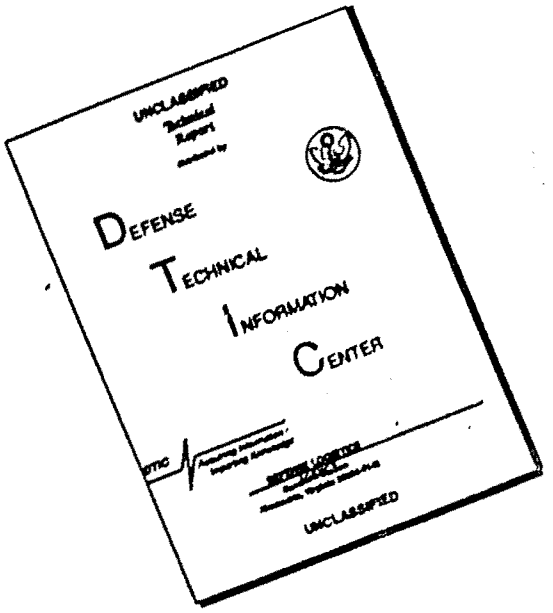

THIS DOCUMENT IS BEST QUALITY AVAILABLE. THE COPY FURNISHED TO DTIC CONTAINED A SIGNIFICANT NUMBER OF PAGES WHICH DO NOT REPRODUCE LEGIBLY.

AFCRL-64-292 March 1964

SCIENTIFIC REPORT NO. 1

TRANSVERSE FOCAL REGION OF A SPHERICAL REFLECTOR

Part 1: Geometric Optics

BY ROY C. SPENCER AND GEOFFREY HYDE

CONTRACT NO. AF 19(628)2758

PROJECT NO. 4600, TASK NO. 460007

RADIO CORPORATION OF AMERICA
MISSILE AND SURFACE RADAR DIVISION
MOORESTOWN, NEW JERSEY

PREPARED FOR

AIR FORCE CAMBRIDGE RESEARCH LABORATORIES
OFFICE OF AEROSPACE RESEARCH
UNITED STATES AIR FORCE
BEDFORD MASSACHUSETTS

AFCRL CONTRACT MONITOR: OTHO KERR

ABSTRACT

The concepts of geometric optics as applied to a spherical reflector are discussed in detail. The caustic surface of a spherical reflector is examined, with particular emphasis on the advantages of complex number notation, and representation in terms of the height of the incoming ray and the arc length along the caustic. The focal region within the caustic curves is studied, and the importance of the circle of least confusion is pointed out. The use of wavefront constructions as an alternate approach is illustrated. The functional relationships are developed for the path-length to a field point on a concentric surface in the focal region, its spherical coordinates, and the height of incoming rays. Computations are summarized on graphs. Finally, the relationship between stationary phase and path-length is mentioned.

SUMMARY

This report covers the application of geometric optics to the problem of the transverse antenna feed for a spherical reflector being studied under contract AF19(628)2758, "Transverse Antenna Feeds". It begins with an introduction to the geometric optics of a spherical reflector, covering the justification of studying rays only in a single plane, and a review of the classical aberrations. This is followed by a detailed treatment of the caustic surface. The historical and mathematical background of the caustic is briefly reviewed. Photographs of caustics are shown. The derivation of the caustic and its properties in terms of complex numbers is studied, including formulas for points on a caustic, arc length (which is related to phase along the caustic), radius of curvature and the evolutes of the caustic. The displacement h, of an incoming ray from the center of the sphere turns out to be useful as a variable. The representation of some of the important quantities in terms of h, and in terms of s, the distance along the caustic is then developed, and in some cases graphed. Because all reflected rays pass through it and because of its small size, the circle of least confusion is studied as a potential feed surface for the spherical reflector, using both graphical and analytical methods. The approach to the problem of the spherical reflector through wavefront analysis is discussed. This method is demonstrated by construction of three sets of wavefronts near the caustic and by construction of wavefronts by transmission from the sphere. Pathlength to field points in the focal region is then studied. L, the pathlength to, and θ_p, the angular location of a field point are computed and graphed against h as independent variable and against each other, with r_p, the radius vector to the field point as a varying parameter. The derivatives dL/dh and $d\theta/dh$ are also plotted. These curves are reviewed, bringing out in particular the existence of up to three rays at any field point and the variation of path-length within the caustic surface. Last, the relationship of path-length to future work using the method of stationary phase is pointed out.

TABLE OF CONTENTS

LIST OF FIGURES

1.0 INTRODUCTION

This report is Part I of a study for AFCRL on Contract AF19(628)2758 "Transverse Antenna Feeds". The purpose of the study is first, to evaluate the electromagnetic field in the focal region of a spherical reflector and second, to design a transverse antenna feed array that will correct for the inherent spherical aberration of the sphere and provide limited beam scanning at microwave frequencies.

Part I considers those geometric concepts which will be used in the solution, namely, ray tracing, optical path lengths, description of the focal region, information on the circle of least confusion, and elementary Huygens' wave theory. Part II will consider the polarization of the induced surface currents and of the reflected waves required to evaluate the strong cross polarization components of the field. A later report will deal with the evaluation of the focal region by the method of stationary phase. Theoretical results will be checked by experimental measurements in the focal regions of a circular pillbox reflector and a spherical reflector.

Electromagnetic field problems as complex as this one have always resisted efforts at rigorous solution. Invariably, simplifying assumptions or approximations must be made in order to obtain realistic answers.[1,2] In this respect simplification is realized and significant results obtained using geometric optics, where the important assumption is that wavelength is small, i.e. $\lambda \longrightarrow 0$. Geometric optics leads to the concept of propagation along rays and thence to the use of ray tracing and geometry as the principal analytical tools. Application of these tools leads to the study of image formation, of focussing and of aberrations. And it is here, in the study of the focussing properties of the spherical reflector, for a point object or target at a great distance, that we have concentrated our efforts. This report discusses in detail the results of these efforts.

Geometric optics has its limitations. It does not account for polarization effects, or diffraction. Some aspects of these are treated in later parts of this study, as indicated earlier. The insight gained from geometric optics into the focal region, in particular, the existence of up to three rays at any point in the focal region, and the path length calculations, has given direction to the effort in the later phases, especially the stationary phase evaluation, which is strongly related qualitatively to this earlier work.

2.0 REVIEW

The sphere is the simplest of all three-dimensional surfaces because its radius of curvature is constant. Consequently, it has no preferential direction and every radius (or normal) passes through its center and is an axis of symmetry. Also, every plane section through the center is a great circle. These properties will now be applied to the optics.

Consider a parallel pencil of rays incident on the concave side of a spherical cap as in Figure 1. The optics is simplified if the incident ray through the center O of the sphere, the central ray, is chosen as the axis. The law of reflection states, (a) that the reflected ray lies in the plane of incidence (the plane containing the normal to the surface, OB and the incident ray AB), and (b) that the angle of reflection equals the angle of incidence. The plane of incidence therefore contains the center, which lies on the normal, as well as the axis, and intersects the sphere in a great circle. It follows that (a) all problems of reflection of a single ray reduce to that of reflection from a circle; and (b) all reflected rays intersect the axis. There can therefore be no skew rays (rays that miss the axis), as there are in the off-axis illumination of the paraboloid. It further follows that all incoming linearly polarized waves are treated alike.

Incoming rays, parallel to and very near the ray passing through the center of the sphere, pass through a focus F called the paraxial focus located half-way down the

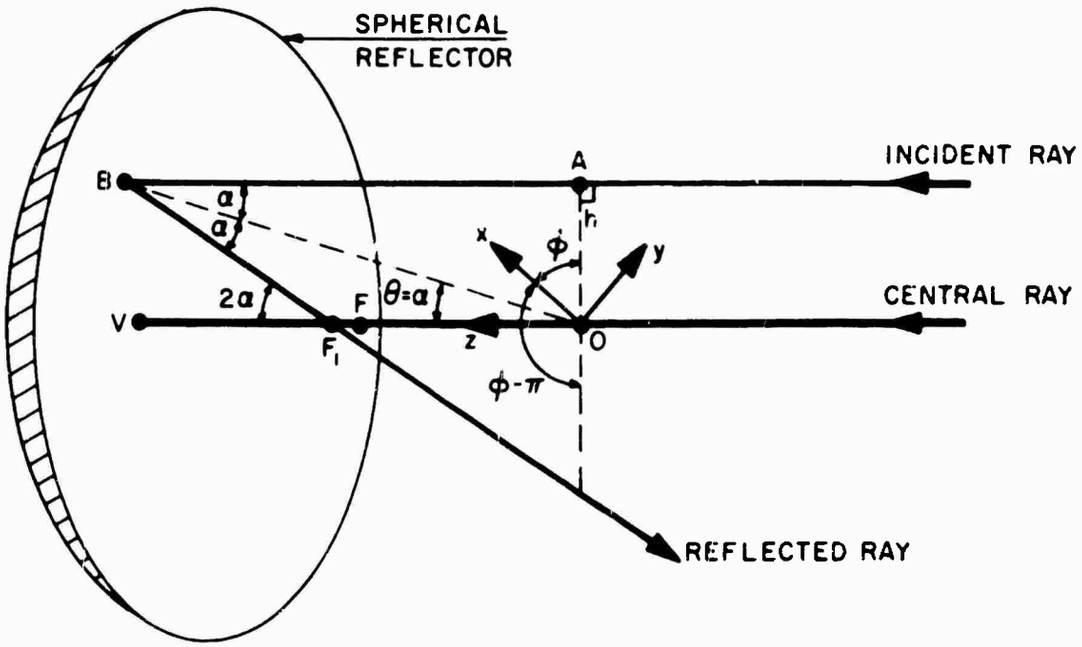

Figure 1. Spherical Cap and Incident and Reflected Ray

central ray from the center of curvature to the spherical reflector. In general, for any doubly curved reflector all reflected rays are tangent to two caustic surfaces. A caustic is defined as the envelope of reflected (or refracted) rays as the position of the point of incidence is varied. It is a region of high energy density. All rays incident on the reflector the same distance from the central ray, upon reflection intersect at the same point on this ray. This point moves from the paraxial focus toward the vertex as the incident rays go from the central ray outwards, thus forming a line, the axial caustic, which is a degenerate caustic surface. All reflected rays intersect this line.

Consider now a typical ray AB incident on the spherical reflector at B (see Figure 1). It is parallel to the central ray and separated from it by a distance h. Let the center of the sphere (center of curvature of the reflector) be O, the point of incidence of the central ray on the reflector be V, and the co-ordinate system have its origin at O and axes as shown. Then h is the length $|\overrightarrow{OA}|$, where A is the foot of the perpendicular from O. Let the angle between the incident ray and the normal, $\measuredangle$ ABO, be α. Then by the laws of reflection noted earlier the angle of reflection $\measuredangle$ OBF$_1$ is also α, and further, the reflected ray, the normal and the incident ray all lie in the same plane, i.e., points O, B, A lie in the plane of incidence. But AB is parallel to OV, therefore the plane contains the central ray, and further, the co-ordinate angle θ of the point B equals α. Thus the reflected ray must intersect OV, say at F$_1$. In terms of our co-ordinate system, since the z axis lies along the central ray, $\overrightarrow{OA}$ lies in the x-y plane, at angle ϕ with respect to the x-axis, and the plane of incidence is characterized by the angles ϕ and $\phi-\pi$. The other two important parameters are h and θ (or α).

There is no loss in generality if we let $\phi = 0$, as in Figure 2. Here again $\theta = \alpha$, and the reflected ray makes an angle 2α with the central ray. Since triangle OF$_1$B is isosceles,

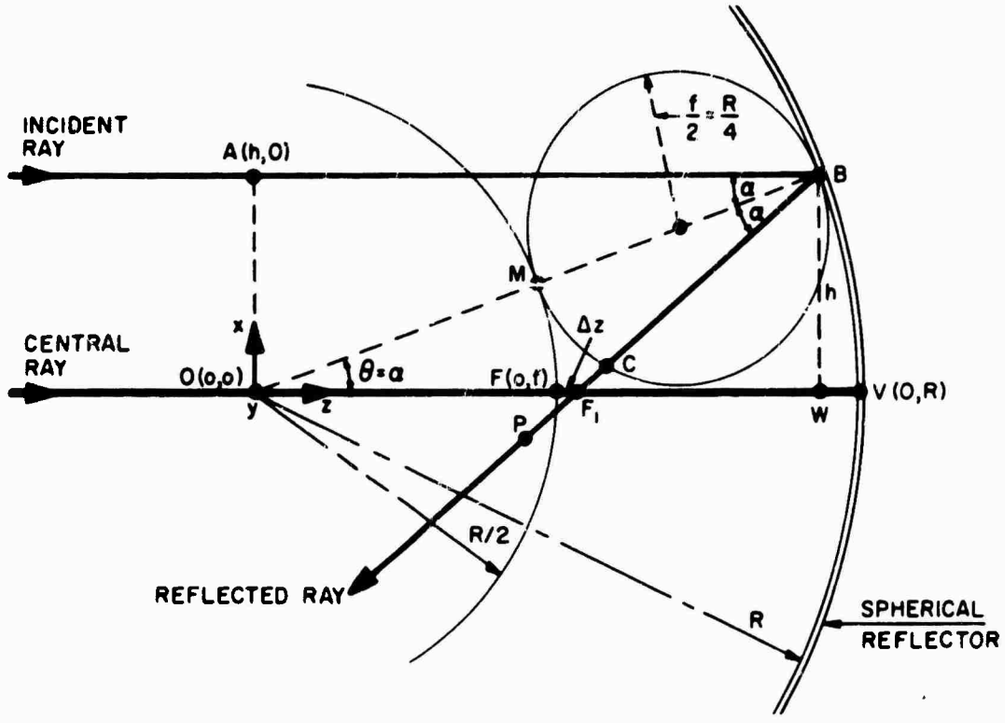

Figure 2. Geometry of Circular Section

$$OF_1 = OM \sec\alpha$$

but

$$OM = R/2 = f$$

Hence

$$OF_1 = f + \Delta z = f \sec\alpha \qquad (1)$$

For $\alpha = 0$, $OF = f = R/2$, i.e., in the limit of rays near the central ray, OF_1 approaches R/2. These rays are termed paraxial rays and F is termed the "paraxial focus".

The shift in the intercept with the central ray from F to F_1 is

$$\Delta z = F_1 - F = f(\sec\alpha - 1) \qquad (2)$$

and is termed the "longitudinal spherical aberration."[3] This and other useful information on path-lengths, phase errors, etc. are discussed by Spencer, Sletten and Walsh[4], who studied the phase along the axis of the sphere. This study was later incorporated in the design of the 1000 foot diameter spherical reflector with corrected line source feed at Arecibo, Puerto Rico.

Since the incoming rays are incident at an angle to the normal, their images suffer from the usual astigmatism. Thus, a narrow bundle of rays close to AB but in the plane of Figure 2 will focus at C, a point on the circle BCM of diameter f. The "tangential" focal length is:

$$BC = BM \cos\alpha = f \cos\alpha \qquad (3)$$

On the other hand, the fan of rays perpendicular to the plane of the figure intersects at F_1 on the axis. Thus the "sagittal" focal length is given by:

$$B F_1 = f \sec\alpha \qquad (4)$$

Its magnitude equals that for OF_1, Eq. (1). The difference CF_1 between the sagittal and tangential focal lengths is the astigmatism of the reflector element at B. Note that the geometric mean of the two focal lengths is simply f.

3.0 THE CAUSTIC SURFACE

3.1 Generation of the Caustic Surface

The locus of C in Figure 2 is an epicycloid termed the "Nephroid". Kinematically, it can be generated by a point C on a sphere of diameter BM = f = R/2, rolling about a sphere of radius OM = f = R/2. When the curve C is revolved about the axis OV we obtain a caustic surface which is a surface of revolution. Historical background and collections of pertinent formulas are to be found in the Encyclopedia Brittanica[5], Yates[6] and Zwikker[7]. Interestingly, much of the mathematics associated with the reflection of rays (and waves) from spheres was known by Huygens in 1679, almost 300 years ago, when he introduced the concept of what is now known as "Huygens' Wavelets". A wave treatment of the region between the caustics is described briefly in Section 4 of this report.

Traces of caustic surfaces formed by reflection or refraction can be observed in everyday life. Figure 3 shows a reflected caustic in a bowl partially filled with milk. The cusp is clearly observed. Figure 4 shows caustics formed by a plastic cylinder filled with water. The caustic by reflection was formed by light that entered through the top surface. The caustic by refraction was formed by light entering the right side of the cylinder and emerging on the left.

Let us now consider a family of parallel rays, i.e., a bundle of rays, traced through reflection from a spherical reflector. A plane section is shown in Figure 5. It is evident that the reflected rays fold into a sort of a fan whose envelope is densely populated by rays. This is the caustic curve. It is formed by the crossing of adjacent rays in a plane.

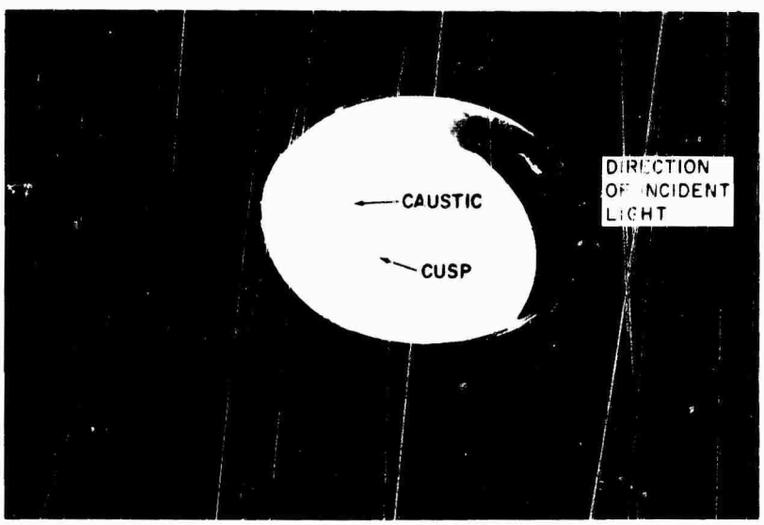

Figure 3. Photograph of Caustic in a Bowl of Milk

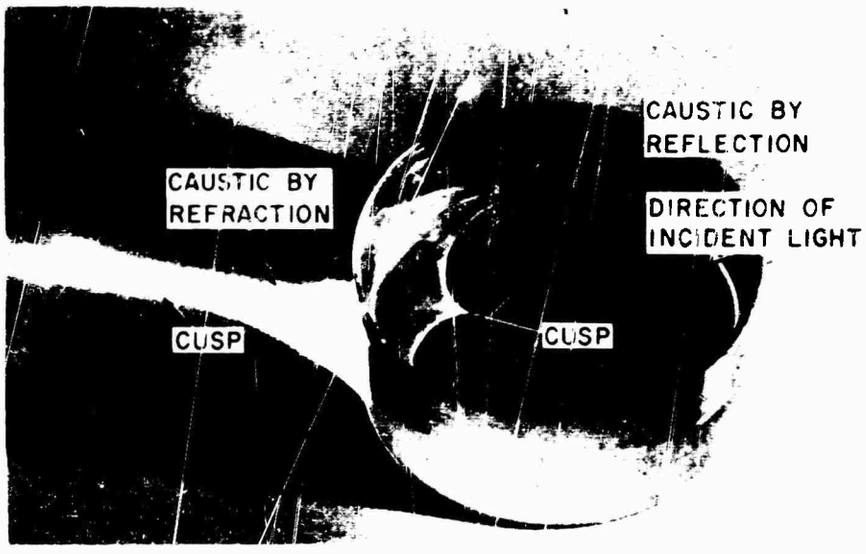

Figure 4. Photograph of Caustics by Reflection and Refraction

3.2 Use of Complex Number Notation

3.2.1 Reflected Rays

Reflection of rays from surfaces can be handled by vector analysis or by the differential equations of envelopes. In our case it is simpler to carry out the analysis by use of complex number representation[7] in the plane of incidence. Consider in Figure 6 a sphere of unit radius (R = 1.0). The unit vector, $e^{i\alpha}$, indicates the normalized position vector OB for a point on the sphere. A position vector OQ connecting the center of the sphere to a point on the reflected ray is then represented by

$$\vec{r} = \vec{OQ} = \vec{OB} + \vec{BQ}$$

i.e.

$$\vec{r} = e^{i\alpha} - p\, e^{2i\alpha} \tag{5}$$

where p is the scalar distance BQ along the reflected ray.

When p intersects the axis, Q is coincident with F_1 and the imaginary part of Equation (5) is zero.

$$0 = \sin\alpha - p \sin 2\alpha$$

On dividing by $\sin\alpha$ and transposing,

$$p = \frac{1}{2} \sec \alpha \tag{6}$$

This is the value of BF_1 which checks with Equation (4).

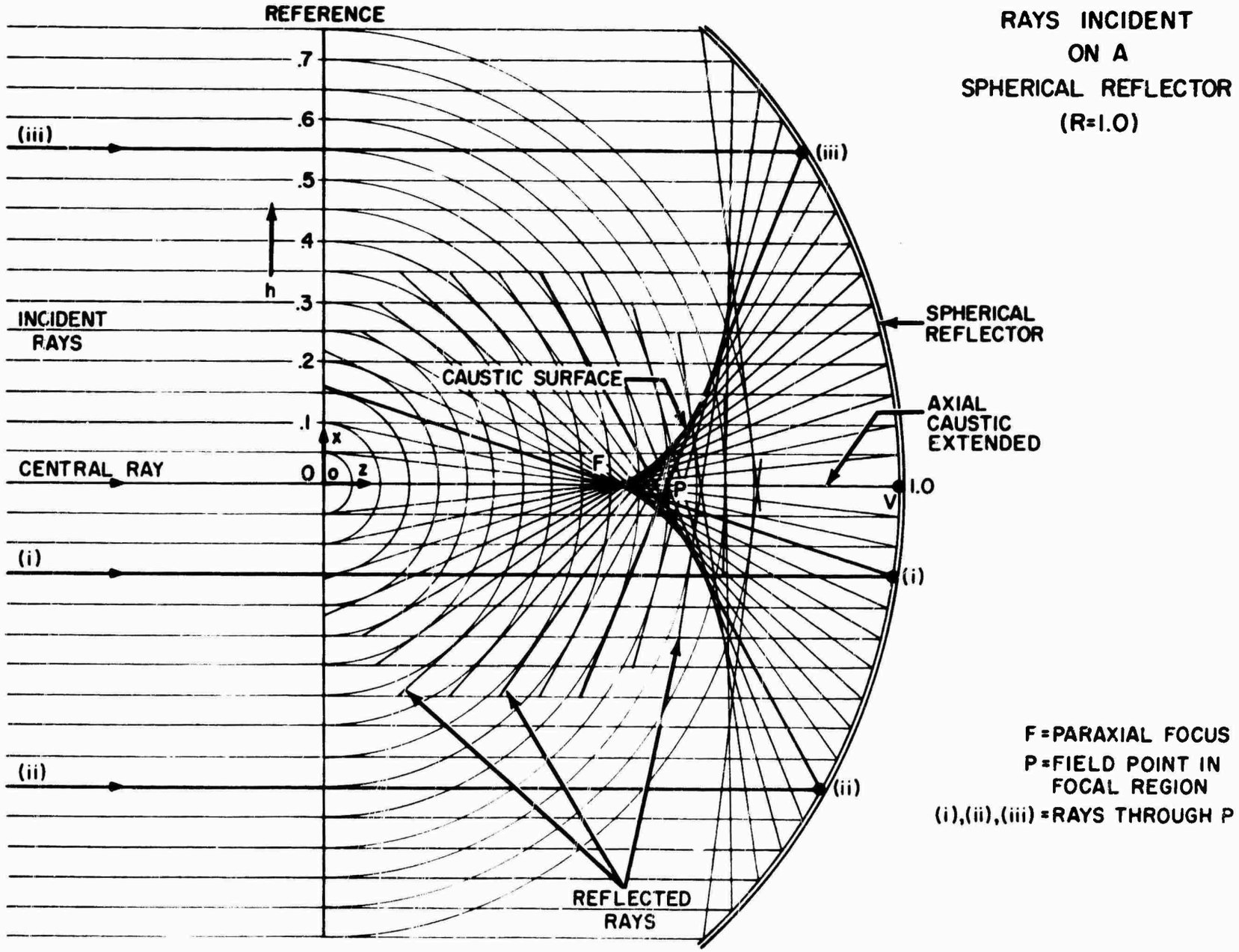

Figure 5. Caustic by Geometric Ray Tracing

COMPLEX NUMBER NOTATION

$$\vec{r} = e^{i\alpha} - pe^{2i\alpha}$$

$$BC = f \cos\alpha = \frac{1}{2}\cos\alpha$$

$$\frac{ds}{d\alpha} = \frac{3}{2}\sin\alpha$$

$$OA = \sin\alpha = h$$

$$AB = \cos\alpha$$

$$OF = f = \frac{1}{2}$$

$$OF' = \frac{1}{2}\sec\alpha$$

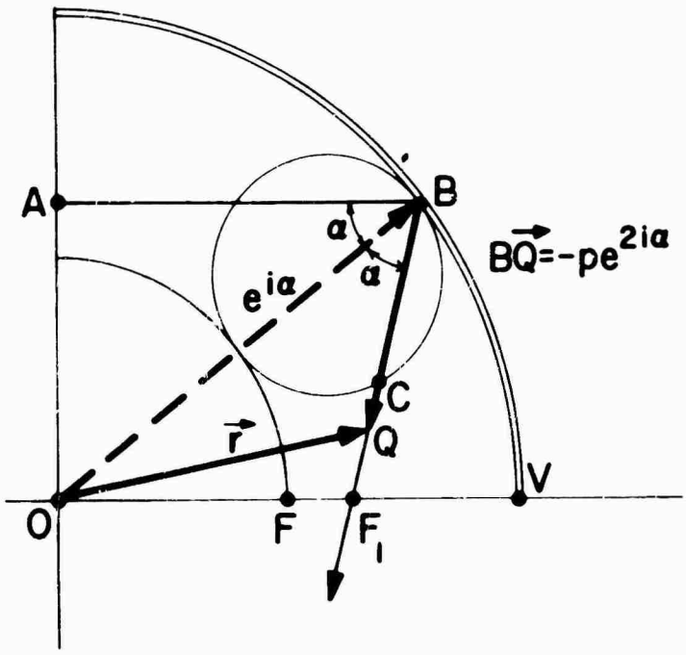

Figure 6. Geometry of Reflection (Complex Number Notation)

3.2.2 Point on Caustic

A caustic is by definition the envelope of reflected (or refracted) rays, as the position of the point of incidence is varied. Differentiation of Equation (5) with respect to α yields

$$\frac{d\vec{r}}{d\alpha} = i\,e^{i\alpha} - 2\,ip\,e^{2i\alpha} - e^{2i\alpha}\,\frac{dp}{d\alpha}$$

$$= e^{2i\alpha}\left[\underset{\text{imaginary}}{i(\cos\alpha - 2p)} + \underset{\text{real}}{\sin\alpha - \frac{dp}{d\alpha}}\right] \qquad (7)$$

For Q to coincide with C, a point on the caustic, $d\vec{r}/d\alpha$ must be parallel to $e^{2i\alpha}$ so that the imaginary part within the square brackets of Equation (7) is zero. Thus

$$p = \frac{1}{2}\cos\alpha = f\cos\alpha \qquad (8)$$

which checks with Equation (3).

The real part in the brackets of Equation (7) is $ds/d\alpha$, the rate of variation of s, the arc length of the caustic. To evaluate this, one differentiates Equation (8) to obtain

$$\frac{dp}{d\alpha} = -\frac{1}{2}\sin\alpha \tag{9}$$

which is then substituted into the real part of Equation (7). The result is

$$\frac{ds}{d\alpha} = \frac{\left|d\vec{r}_c\right|}{d\alpha} = \frac{3}{2}\sin\alpha \tag{10}$$

An alternate expression for a point C on the caustic arises from the fact that C is on the circle of diameter MB (see Figure 7). We may then represent its position vector by

$$\vec{OC} = \vec{r}_c = \vec{OB'} + \vec{B'C}$$

$$\vec{r}_c = \frac{3}{4}e^{i\alpha} - \frac{1}{4}e^{3i\alpha} \tag{11a}$$

The real and imaginary portions of this yield the classical coordinates of the caustic with respect to the origin O. If

$$\vec{OC} = z_c + i\,x_c \tag{11b}$$

then

$$4z_c = 3\cos\alpha - \cos 3\alpha$$

$$4x_c = 3\sin\alpha - \sin 3\alpha$$

These equations can be transformed to

$$2z_c = \cos\alpha\left[1 + 2\sin^2\alpha\right] \tag{12a}$$

$$x_c = \sin^3\alpha \tag{12b}$$

Differentiation of Equation (11a) yields

$$\frac{d\vec{r}_c}{d\alpha} = i\,\frac{3}{4}\left[e^{i\alpha} - e^{3i\alpha}\right]$$

$$r_c = \frac{3}{4} e^{i\alpha} - \frac{1}{4} e^{3i\alpha}$$

$$4z_c = 3\cos\alpha - \cos 3\alpha$$

$$4x_c = 3\sin\alpha - \sin 3\alpha$$

$$s = \frac{3}{2}(1-\cos\alpha)$$

$$\rho = \frac{1}{2}\frac{ds}{d\alpha} = \frac{3}{4}\sin\alpha$$

$$z_c = \frac{1}{2}\sqrt{1-h^2}\left[1+2h^2\right]$$

$$x_c = h^3$$

$$4r_c^2 = 1+3h^2$$

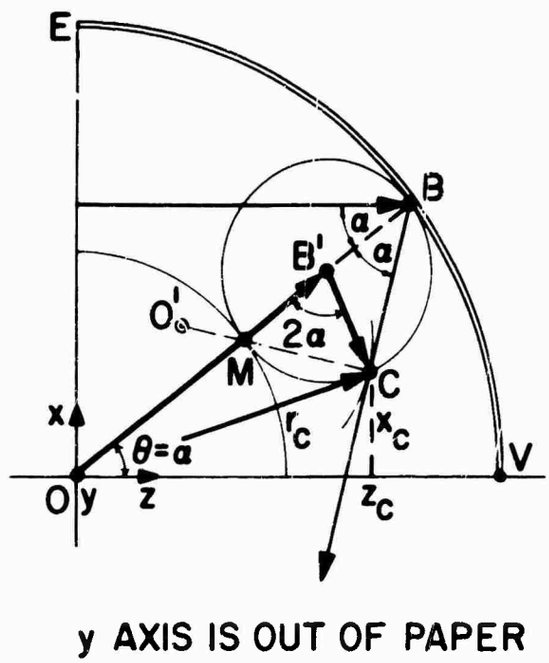

Figure 7. Geometry of Reflection (Alternate Representation)

Whence

$$\frac{d\vec{r}_c}{d\alpha} = \frac{3}{2} e^{2i\alpha} \sin\alpha \tag{13}$$

But $d\vec{r}_c/d\alpha$ can also be expressed as

$$\frac{d\vec{r}_c}{d\alpha} = e^{2i\alpha} \frac{ds}{d\alpha} \tag{14}$$

By comparison of Equations (13) and (14):

$$\frac{ds}{d\alpha} = \frac{3}{2}\sin\alpha \tag{15}$$

which checks with Equation (10).

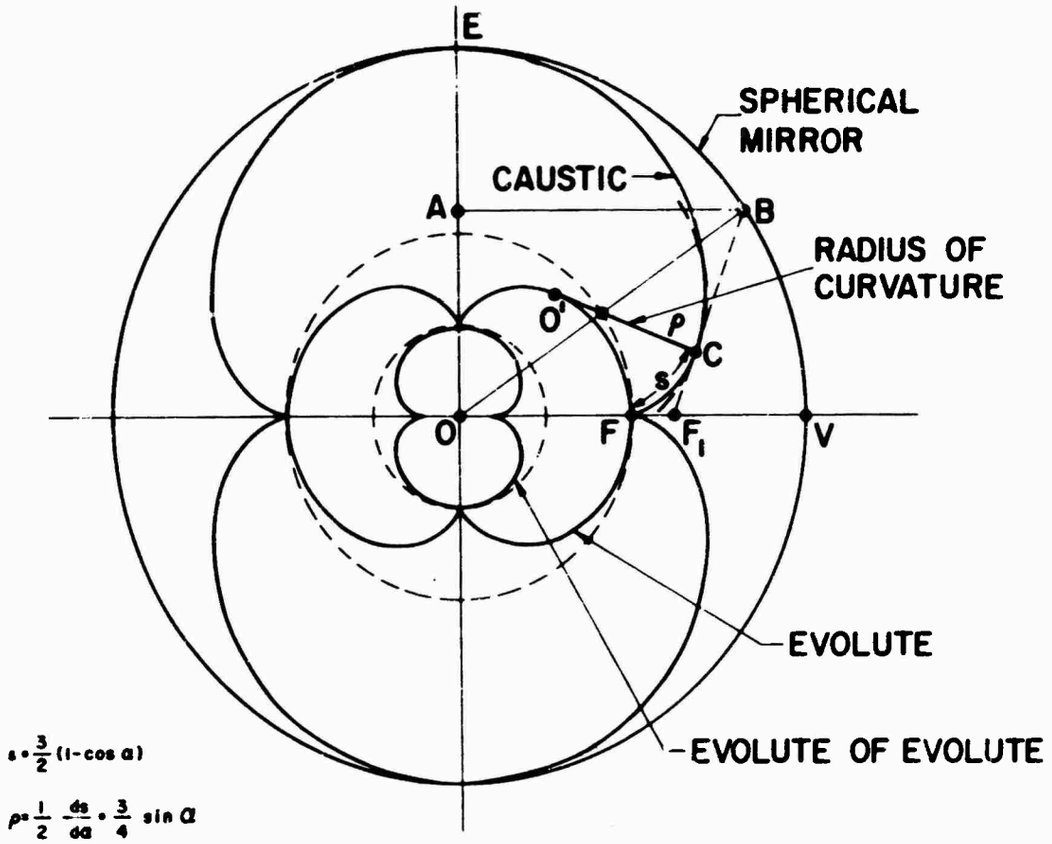

Figure 8. Evolutes of the Caustic

3.2.5 Evolute of Caustic

The evolute of any curve is the locus of centers of curvature. It has the property that, if a string is unwrapped from the evolute, a point on the string will generate the curve, or a parallel curve, depending on the initial length of the string. It is known that the evolute of any epicycloid[10] is a similar epicycloid but rotated so that its cusps lie midway between those of the epicycloid. In particular, the evolute of the caustic of the sphere (for the source point at infinity) is a similar epicycloid but to half the scale, and rotated 90°. This is shown in Figure 8. Shown also is the evolute of the evolute of the caustic. This is concentric with, and similar to, the caustic but to one fourth its scale.

3.2.6 Anticaustic

If a string is tied to a point source and then stretched around a pencil at point B on the reflector Figure 9, and thence to a tangent point C on the caustic and along the arc to F, the pencil will trace the outline of the reflector as it is moved around along the string. The trace of the pencil is called the anticaustic[11]. When applied to the sphere it implies that the sum of the optical path lengths is a constant.

$$\overline{AB} + \overline{BC} + \overset{\frown}{CF} = \overline{OV} + \overline{FV} = 3/2 \qquad (20)$$

where the overhead bar or arc indicate the scalar magnitudes of the corresponding chord or arc length.

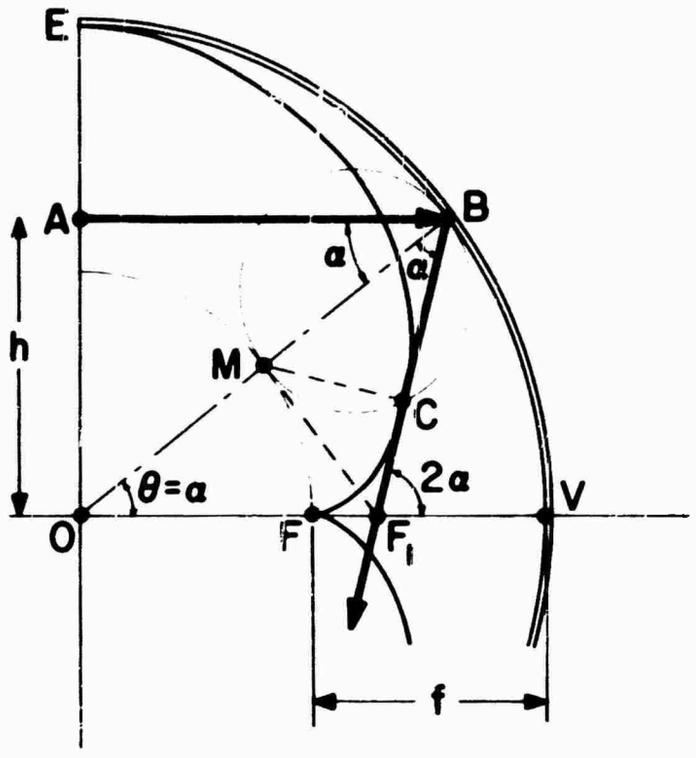

Figure 9. Optical Path-Length and the Anticaustic

3.3 Transformation of Variables

Because of the physical meaning, it is very useful to express formulas in terms of h, and also s, the arc length along the caustic. Because it is the angular co-ordinate of the field point, θ will also be introduced into some formulas in place of α.

3.3.1 h as a Variable

The importance of h, the distance of the incident ray from the central ray, was mentioned earlier. In addition, certain formulas, as well as their expansion in series, are simplified by use of the substitution

$$h = \sin \alpha \tag{21}$$

For example, the radius of curvature ρ of the caustic is given by

$$2\rho = \frac{ds}{d\alpha} = \frac{3}{2} h$$

Then x_c and z_c, coordinates of a point C on the caustic given in Equations (12a) and (12b), transform to

$$2z_c = \left(1 - h^2\right)^{1/2} (1 + 2h^2) \tag{22a}$$

$$x_c = h^3 \tag{22b}$$

An accurate plot of part of the caustic curve is given in Figure 10. On squaring and adding the coordinates we obtain a simple equation for r_c, the radius vector from the center.

$$4r_c^2 = 1 + 3h^2 \tag{23}$$

This is a hyperbola in r_c and h, with $r_c \geq 1/2$.

The equation of the circular arc which is the intersection of the spherical reflector and the x-z plane is $x^2 + z^2 = 1$. (Recall R = 1.0.) All incident rays are parallel to the z-axis. So the incident ray, passing through A at height h has the equation

$$x = h$$

The intersection of the incident ray and the reflector, B, occurs at

$$x = h; \quad z = -\left(1 - h^2\right)^{1/2}$$

As before, ΔOF_1B is isosceles (see Figure 2).

Therefore $F_1B = F_1O$, and from Equations (1) and (21)

$$F_1B = \frac{1}{2\left(1 - h^2\right)^{1/2}} = F_1O$$

Hence the coordinates of the intercept are

$$F_1 = F_1\left(0, \frac{-1}{2\left(1 - h^2\right)^{1/2}}\right)$$

Note that in the limit as $h \to 0$, i.e., for the paraxial rays,

$$F_1 \to F \equiv F\,(0, -1/2)$$

$$h \to 0$$

a familiar formula.

Then x_c and z_c, coordinates of a point C on the caustic given in Equations (12a) and (12b), transform to

$$2z_c = \left(1 - h^2\right)^{1/2} (1 + 2h^2) \tag{22a}$$

$$x_c = h^3 \tag{22b}$$

An accurate plot of part of the caustic curve is given in Figure 10. On squaring and adding the coordinates we obtain a simple equation for r_c, the radius vector from the center.

$$4r_c^2 = 1 + 3h^2 \tag{23}$$

This is a hyperbola in r_c and h, with $r_c \geq 1/2$.

The equation of the circular arc which is the intersection of the spherical reflector and the x-z plane is $x^2 + z^2 = 1$. (Recall R = 1.0.) All incident rays are parallel to the z-axis. So the incident ray, passing through A at height h has the equation

$$x = h$$

The intersection of the incident ray and the reflector, B, occurs at

$$x = h; \quad z = -\left(1 - h^2\right)^{1/2}$$

As before, ΔOF_1B is isosceles (see Figure 2).

Therefore $F_1B = F_1O$, and from Equations (1) and (21)

$$F_1B = \frac{1}{2\left(1 - h^2\right)^{1/2}} = F_1O$$

Hence the coordinates of the intercept are

$$F_1 = F_1\left(0, \frac{-1}{2\left(1 - h^2\right)^{1/2}}\right)$$

Note that in the limit as $h \to 0$, i.e., for the paraxial rays,

$$F_1 \to F \equiv F\,(0, -1/2)$$

$$h \to 0$$

a familiar formula.

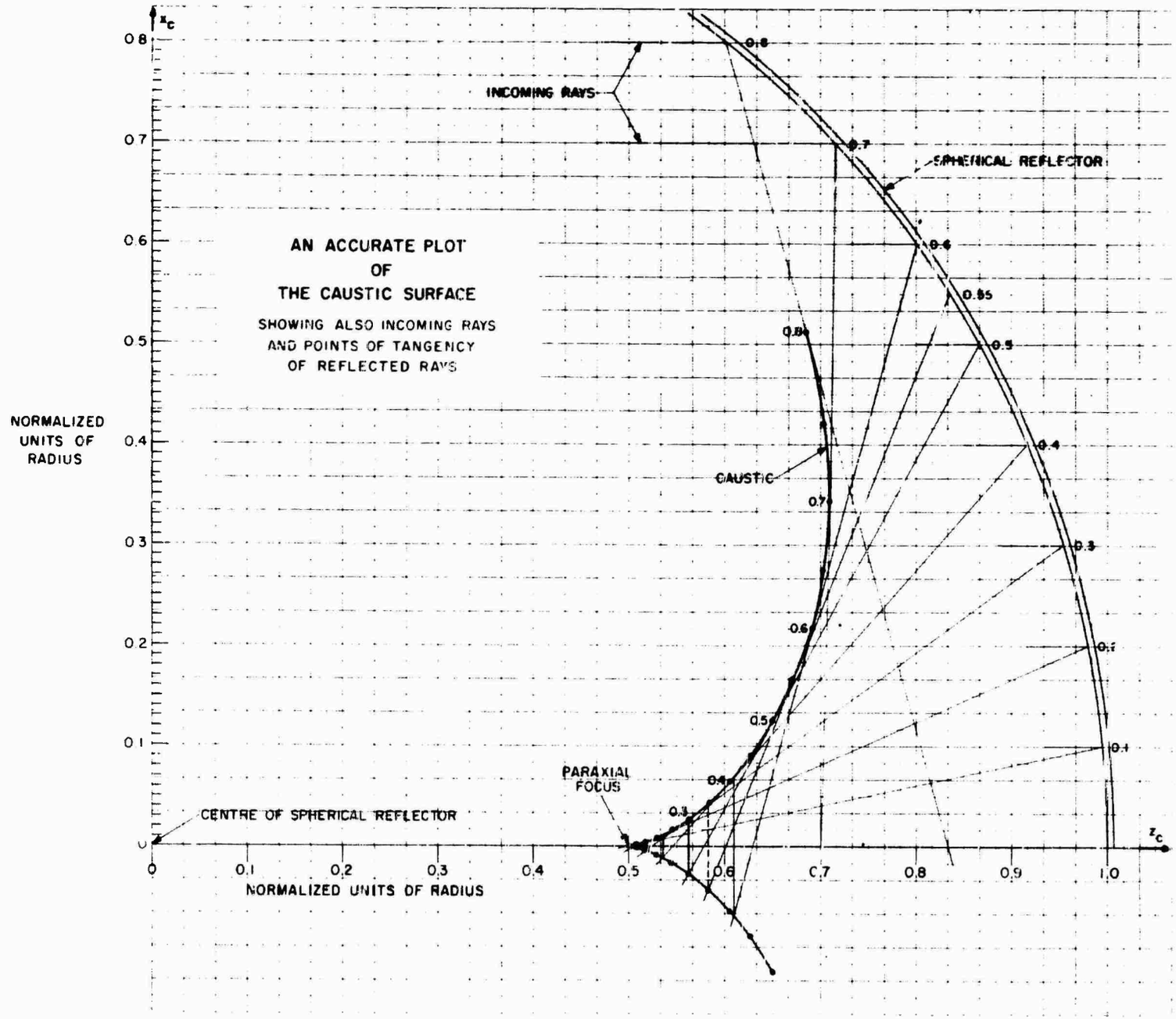

Figure 10. Accurate Plot of Caustic Curve

Sometimes it is useful to express some of these formulas in unnormalized form. It is immediately evident that

$$h = R \sin \alpha = R \sin \theta \tag{21a}$$

$$AB = R \cos \alpha = R \cos \theta = \left(R^2 - h^2\right)^{1/2}$$

$$OF_1 = BF_1 = \frac{-R}{2 \cos \alpha} = \frac{-R}{2 \cos \theta} = \frac{-R^2}{2} \left(R^2 - h^2\right)^{-1/2}$$

Let us consider an arbitrary point, P, lying on the reflected ray.

$P \equiv P(x_p, z_p) \equiv P(r_p, \theta_p)$ and of course, there are constraints on these coordinates. We know the points B and F_1 on this line, so we may write

$$\frac{z_p + \left(R^2 - h^2\right)^{1/2}}{x_p - h} = \frac{\dfrac{-R^2}{2\left(R^2 - h^2\right)^{1/2}} + \left(R^2 - h^2\right)^{1/2}}{-h}$$

or in terms of spherical coordinates

$$x_p = \frac{\sin \theta}{\cos 2\theta} \cdot (-2 z_p \cos \theta + R)$$

and the distance BP is given by

$$BP = \left[x_p^2 + z_p^2 + R^2 - 2R(x_p \sin \theta + z_p \cos \theta)\right]^{1/2}$$

i.e.,

$$BP = \left[R^2 + r_p^2 - 2 R r_p \cos (\theta - \theta_p)\right]^{1/2}$$

It may be noted that [AB + BP] is the path length along the ray from a reference line (perpendicular) through 0, which will be used in the stationary phase derivations of a later report.

3.3.2 Coordinates of Caustic in Terms of s

As a consequence of Equation (20) the phase of any point C relative to F can be obtained by a linear scale for optical path length along the arc FC. In order to construct such a scale and to prepare an accurate template of the caustic, we decided to derive the x and z coordinates in terms of s.

From Equation (16) one may obtain

$$\left(1 - h^2\right)^{1/2} = 1 - \frac{2}{3}\, s$$

On squaring and transposing,

$$h^2 = 4\, \frac{s}{3} - 4\left(\frac{s}{3}\right)^2 \tag{24}$$

On substituting these values into Equation (12a)

$$2 z_c = \left(1 - 2\, \frac{s}{3}\right) \left[1 + 8\, \frac{s}{3}\left(1 - \frac{s}{3}\right)\right] \tag{25}$$

Note that at the cusp F, $s = 0$ and $z_c = 1/2$. When $s = 3/2$ the first factor is zero, making z_c zero. By symmetry, z_c is equal to $-1/2$ when $s = 3$.

One can expand Equation (25)

$$2 z_c = 1 + 6\left(\frac{s}{3}\right) - 24\left(\frac{s}{3}\right)^2 + 16\left(\frac{s}{3}\right)^3$$

and then differentiate

$$\frac{dz_c}{ds} = +1 - 8\, \frac{s}{3} + 8\left(\frac{s}{3}\right)^2 \tag{26}$$

This equals unity when $s = 0$ or 3 but equals -1 when $s = 3/2$. At each of the three points the caustic is parallel to the axis. The derivative Equation (26) is zero when $\alpha = 45^o$.

The value of x_c is given by raising Equation (24) to the 3/2 power

$$x_c = h^3 = 8\left(\frac{s}{3}\right)^{3/2} \cdot \left(1 - \frac{s}{3}\right)^{3/2} \tag{27}$$

One notes the natural occurrence of the variable $s/3$.

Differentiation gives

$$\frac{dx_c}{ds} = 4\left[\frac{s}{3}\left(1 - \frac{s}{3}\right)\right]^{1/2} \cdot \left(1 - 2\, \frac{s}{3}\right) \tag{28}$$

Finally,

$$\frac{d^2 z_c}{ds^2} = -\frac{8}{3}\left(1 - 2\, \frac{s}{3}\right) \tag{29}$$

and

$$\frac{d^2x_c}{ds^2} = \frac{2}{3} \cdot \frac{1 - 8\left(\frac{s}{3}\right) + 8\left(\frac{s}{3}\right)^2}{\left[\frac{s}{3}\left(1 - \frac{s}{3}\right)\right]^{1/2}} \tag{30}$$

In terms of polar coordinates from Equation (23)

$$r_c = \frac{1}{2}\left(1 + 3h^2\right)^{1/2}$$

and now $\theta_c = \sin^{-1}(x_c/r_c)$

Therefore $\theta_c = \sin^{-1}\left[2h^3\left(1 + 3h^2\right)^{-1/2}\right]$

or in terms of s

$$r_c = \frac{1}{2}\left[1 + 12\,\frac{s}{3}\left(1 - \frac{s}{3}\right)\right]^{1/2} \tag{31}$$

$$\theta_c = \sin^{-1} 16\left\{\left[\frac{s}{3}\left(1 - \frac{s}{3}\right)\right]^3 \Big/ \left[1 + 12\,\frac{s}{3}\left(1 - \frac{s}{3}\right)\right]\right\}^{1/2} \tag{32}$$

These functions and their derivatives are shown as functions of s in Figures 11 and 12. Values of r_c and θ_c are plotted for small s in Figure 13. Note that for $s < 0.15$, $z_c \to r_c$ and $x_c/r_c \to \theta_c$. The value of knowing these functions in terms of s arises from the fact that it is demonstrable that phase along the caustic is a linear function of s.

We decided to calculate tables for x_c and z_c for equal increments of $s/3 = 0.001$. These were used to construct a template for a caustic for a circle of radius 100 inches, so that Δs was 0.3 inch. If the division marks represented wavelengths, then there would be 333 1/3 wavelengths in a radius. This was used for the construction of wavefronts as an aid in the analysis of the problem from the wavefront point of view, in Section 4.

3.4 Circle of Least Confusion

In Figure 14, we have drawn a spherical reflector with three rays incident on it. These are the central ray or axial ray, and the edge rays or marginal rays. For our purposes the marginal ray is the outermost ray that is properly reflected. It is characterized by the maximum allowable value of h, h_{max} and the maximum angle of incidence α, α_{max}. The axial caustic, the caustic surface and the paraxial focus are all indicated and have been previously discussed. Now every ray is tangent to the caustic surface. In particular the marginal rays are tangent at the points

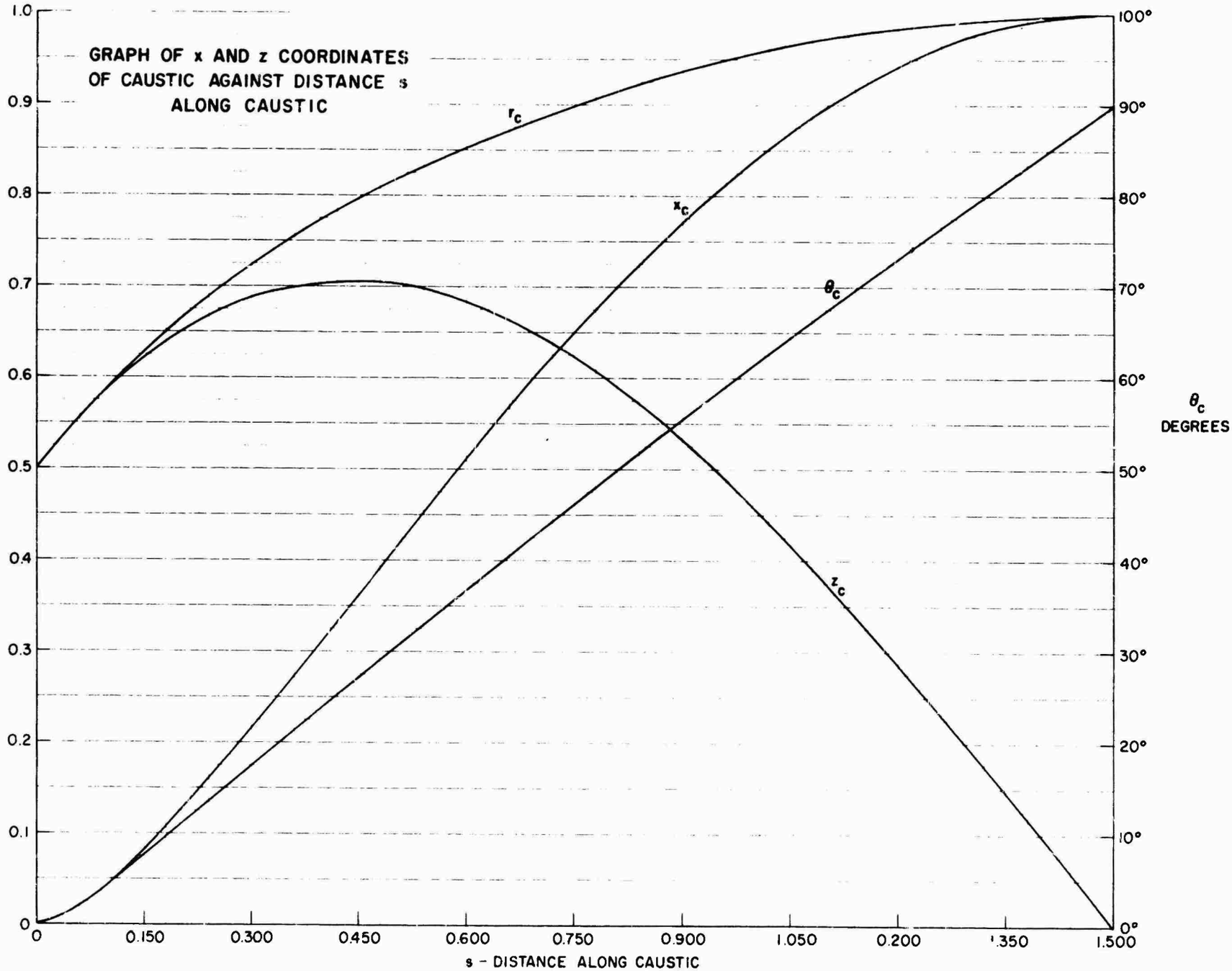

Figure 11. Coordinates of Caustic versus Arc Length

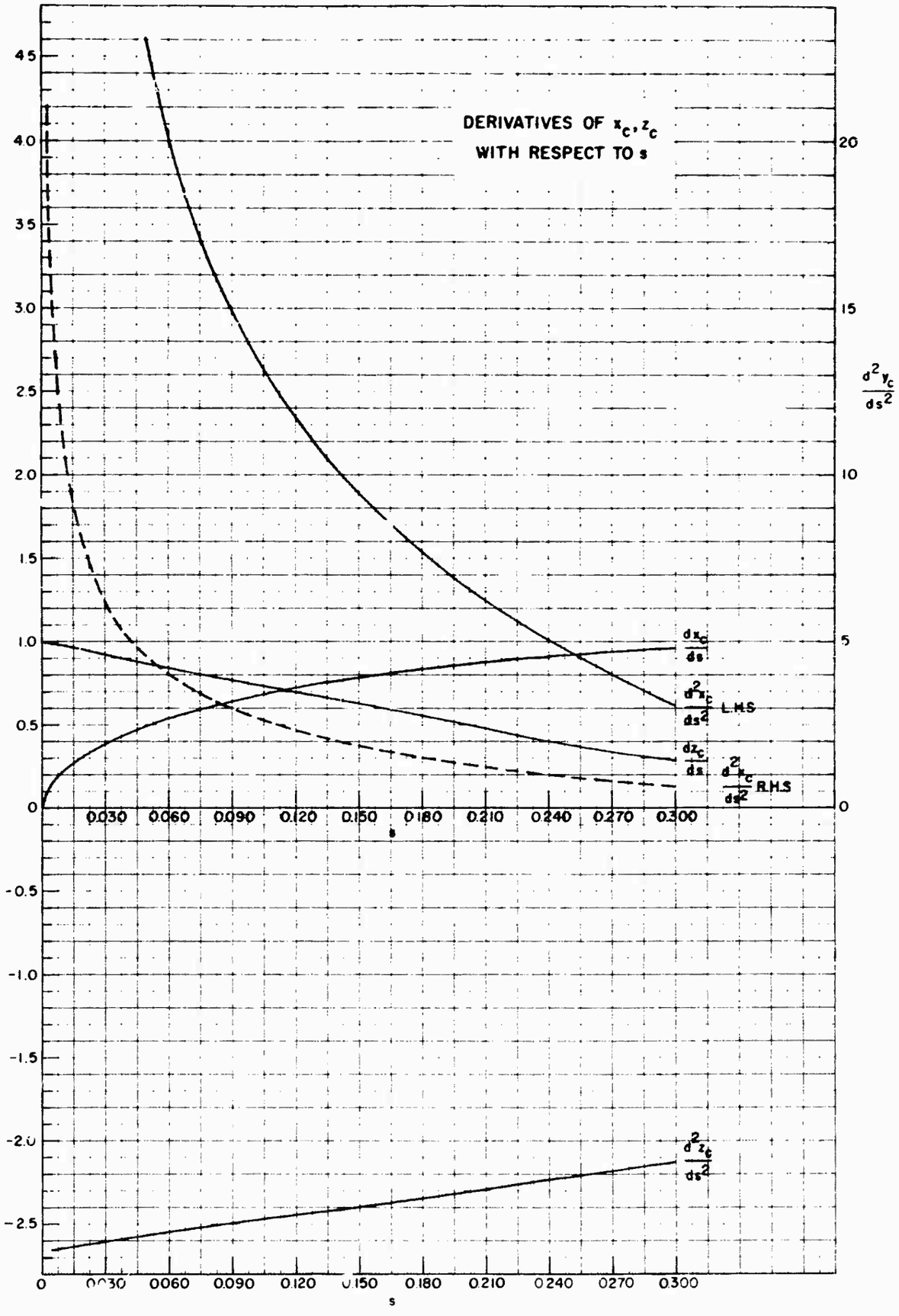

Figure 12. Derivatives of Caustic Coordinates versus Arc length

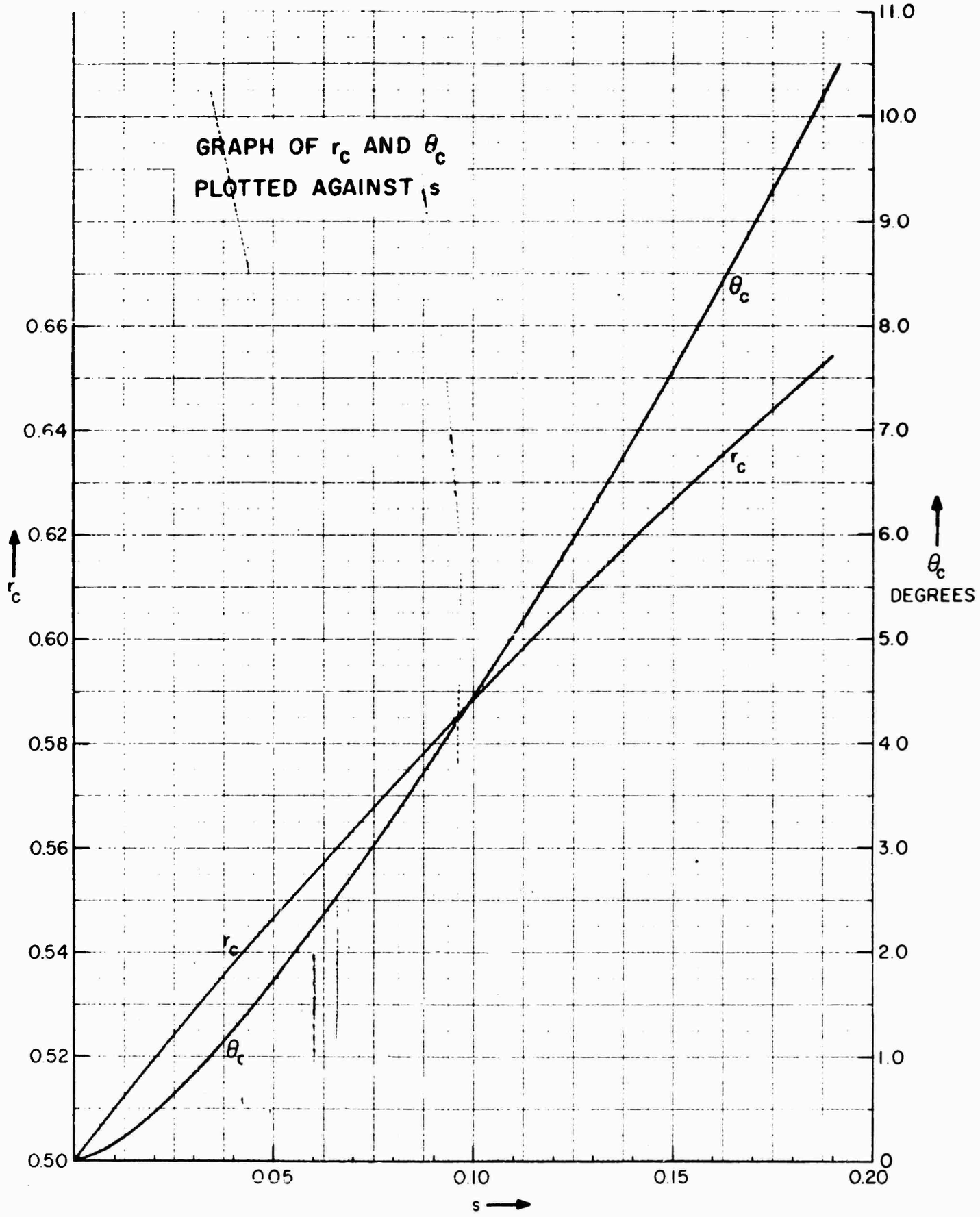

Figure 13. Graph of r_c and θ_c Plotted Against s

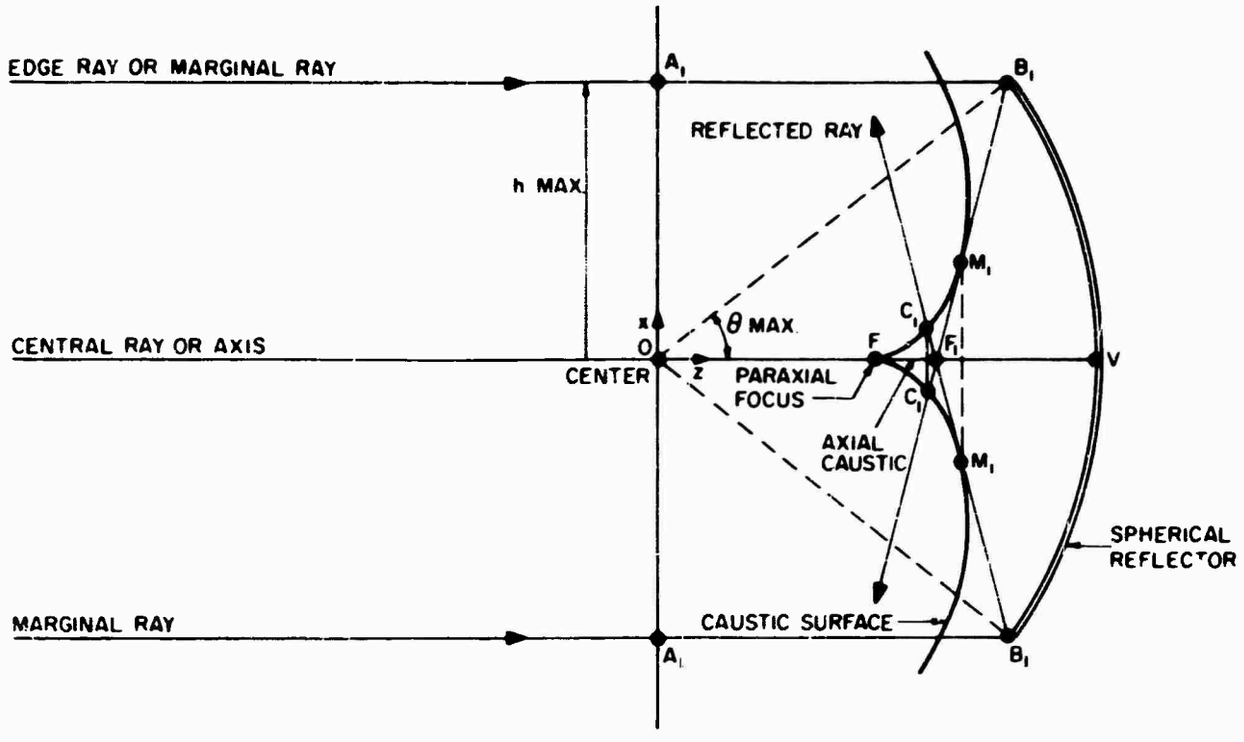

Figure 14. Focal Region of a Sphere

M_1. M_1M_1 is termed the marginal focus. The marginal rays intersect on the axis at F_1 and then intersect the caustic surface a second time at the points C_1. It follows that a circle of diameter C_1C_1 is the smallest circle that contains all the rays. It is termed "the circle of least confusion". For our purposes the region lying between the caustic surfaces and between the paraxial focus and the marginal focus is the focal region, and it is here that we ultimately must concentrate our efforts.

Considering questions of aperture blocking, etc., it would seem reasonable to investigate the region near the circle of least confusion as a potential position for the feed system feeding a spherical reflector. This region is shown enlarged in Figure 15. Since the dimension C_1C_1 is difficult to derive, we will first obtain the diameter of the circle C C which is the same distance r_1 from the center 0 as is the axial intercept F_1. This radius is OF_1, Equations (1) and (21). On squaring OF_1

$$4r_1^2 = \frac{1}{1 - h^2}$$

This can now be compared with Equation (23)

$$4r_1^2 = 1 + 3h_1^2$$

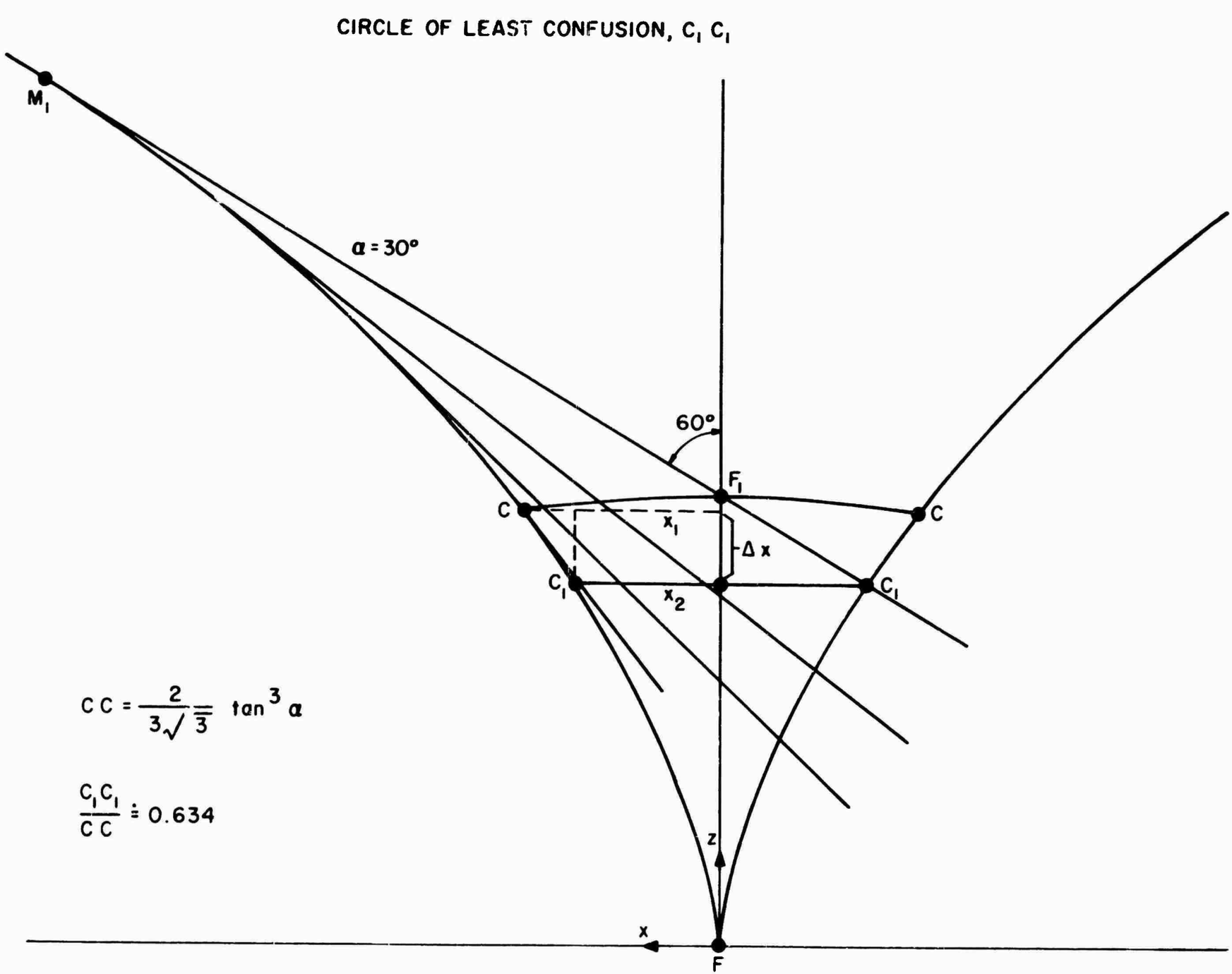

Figure 15. Caustic Region-Circle of Least Confusion

where h_1 corresponds to C. On equating these two and subtracting unity from each side, one obtains

$$3h_1^2 = \frac{h^2}{1 - h^2} = \tan^2 \alpha = t^2$$

so that

$$h_1 = t/\sqrt{3} \tag{33}$$

Note that t is an abbreviation for tan α.

We now substitute Equation (33) in Equation (22b) and obtain

$$x_1 = h_1^3 = \frac{1}{\sqrt{27}} t^3 \tag{34}$$

Example: If $\alpha = 30^o$, $t = 1/\sqrt{3}$ and $x_1 = 1/27$

From Equation (34) a log-log plot of x_1 versus $t = \tan \alpha$ will be a straight line with a slope of 3. This is shown in Figure 16 where the diameter $2x_1$ of the corresponding circle is plotted. The diameter of the circle of least confusion was determined graphically (see Figure 17).

The true circle of least confusion has a somewhat smaller radius x_2. Earlier attempts to approximate it by use of a Taylor's series expansion about the point C failed because such series blow up at the cusp, and the point C_1 was too close to the cusp.

A second attempt was made by linear interpolation from the point C discussed above.

Let the ordinates at C and C_1 be x_1 and x_2 as shown in Figure 15 and let m and m_1 be the slopes of the rays passing through C_1 and C. From Figure 15 we derive the relationships

$$x_2 = m \, \Delta x$$

$$x_1 \doteq (m + m_1) \Delta x \text{ (approximately)}$$

hence

$$x_2 = y_1 \frac{m}{(m + m_1)}$$

Now

$$m = \tan 2\alpha = \frac{2t}{1 - t^2}$$

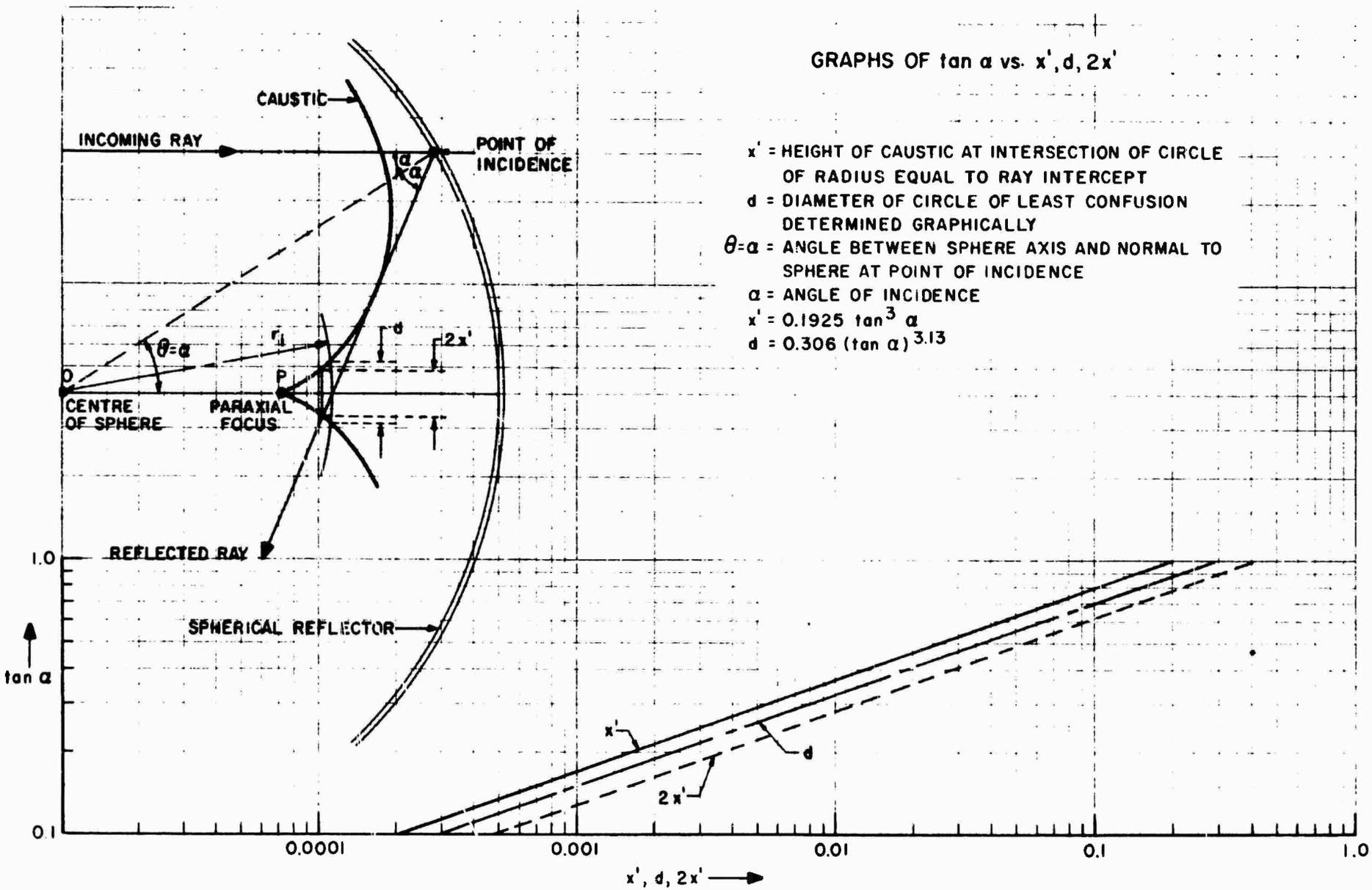

Figure 16. Log-Log Plot of Diameter of Circle of Least Confusion

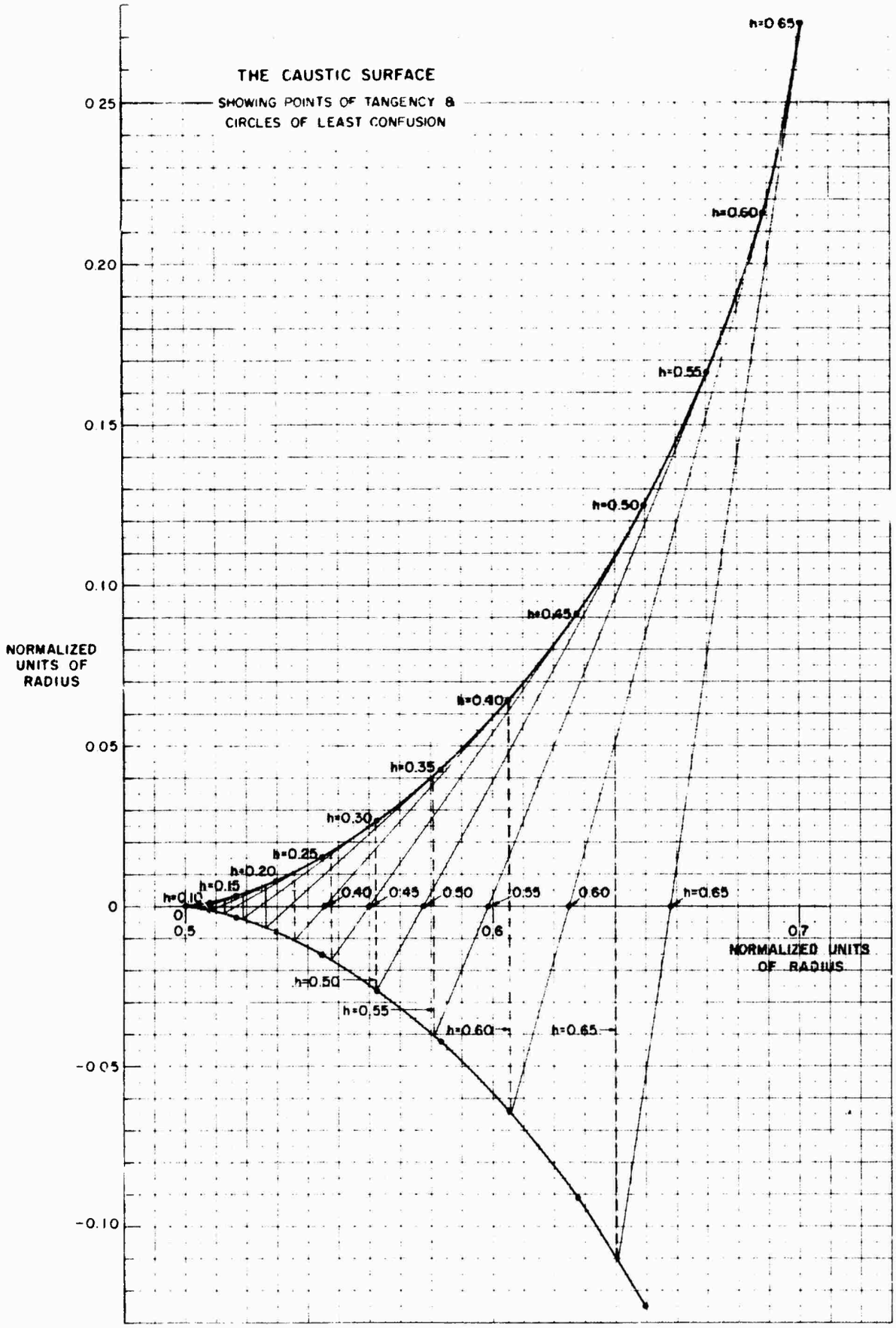

Figure 17. Caustic Surface Showing Tangent Rays and Circles of Least Confusion

For m_1 we use the form

$$m_1 = \tan 2\alpha_1 = \frac{\sin 2\alpha_1}{\cos 2\alpha_1} = \frac{2 h_1 \left(1 - h_1^2\right)^{1/2}}{1 - 2 h_1^2}$$

On substituting from Equation (33) into the above equation,

$$m_1 = \frac{2t}{\sqrt{3}} \frac{\left(1 - \frac{t^2}{3}\right)^{1/2}}{1 - \frac{2}{3} t^2}$$

Dividing results in

$$\frac{m_1}{m} = \frac{1}{\sqrt{3}} \frac{\left(1 - t^2\right)}{\left(1 - \frac{2}{3} t^2\right)} \left(1 - \frac{t^2}{3}\right)^{1/2} \tag{35}$$

This slowly varying function can be approximated by the binomial theorem

$$\frac{m_1}{m} = \frac{1}{\sqrt{3}} \left(1 - t^2\right) \left(1 + \frac{2}{3} t^2 + \ldots\right) \left(1 - \frac{t^2}{6} + \ldots\right)$$

From this

$$\frac{x_2}{x_1} = \frac{m}{m + m_1} = \frac{1}{1 + \frac{1}{\sqrt{3}} \left(1 - \frac{t^2}{2} + \ldots\right)} = \frac{\sqrt{3}}{\left(\sqrt{3} + 1\right) - \frac{t^2}{2} + \ldots}$$

When t is small, then

$$\frac{x_2}{x_1} \doteq \frac{\sqrt{3}}{\sqrt{3} + 1} = \frac{1.73}{2.73} = 0.634 \tag{36}$$

This means that the diameter $2y_2$ of the circle of least confusion is approximately 0.634 times that for the diameter $2x_1$ at the axial intercept F_1. This checks out against the graphical analysis. The measured values of the circle of least confusion should start out proportional to $\tan^3 \alpha$.

4.0 WAVE FRONTS, ORTHOGONAL TRAJECTORIES AND PARALLEL CURVES[12]

4.1 Definitions

These three terms are all equivalent. According to optics, a wave front is the locus of constant phase and, in an isotropic medium, is perpendicular to the rays crossing it. Mathematically, the wave front is the orthogonal trajectory of a set of straight lines, - the curve which crosses each of the lines at an angle of 90^{o}. A bundle of straight lines having this property is said to be orthotomic. An example is a bundle of rays from a point source. Such a bundle of rays remains orthotomic after any number of reflections or refractions from smooth curved surfaces.

A set of equidistant marks along a ray can be used to indicate path-length in wavelengths. Then, as the ray turns so as to coincide with adjacent rays, the points generate a series of parallel curves. Their common evolute is the caustic of the rays. On the other hand, each of the parallel curves is an involute of the caustic.

One method of generating these parallel curves is by tracing the locus of a point on a straight edge which rolls without slipping as a tangent about the caustic. Such a curve is called a roulette.[13] Note that a roulette contains a cusp whenever the point touches the caustic. An equivalent method is to wrap or unwrap a string from the caustic. A point on the string traces the curve which is termed an anticaustic or an involute of the caustic.

4.2 Multiple Nature of Wave Fronts

Such a set of wave fronts or parallel curves is shown in Figure 18. They cross the axis at equidistant intervals and are normal to the caustic, also at equidistant intervals. On reflection from the upper branch of the caustic they generate a second branch of parallel curves. Reflections from the lower branch of the caustic are shown also. Thus at any point within the caustic there is apt to be mutual interference between three sets of waves. The locus of these wave fronts can be computed. The equations were developed but not used as it was decided to actually draw the wave fronts.

The large template for the caustic curve discussed under Section 3.3.2 was augmented by a Leroy lettering pen with finger grip holder attached to a flexible steel tape that was clamped to the caustic curve. By holding the pen holder and tape taut and swinging an arc, a perfect curve was inked directly onto a mylar sheet. After some difficulty in getting used to the unusual gadgetry an excellent set of curves was obtained (Figure 18).

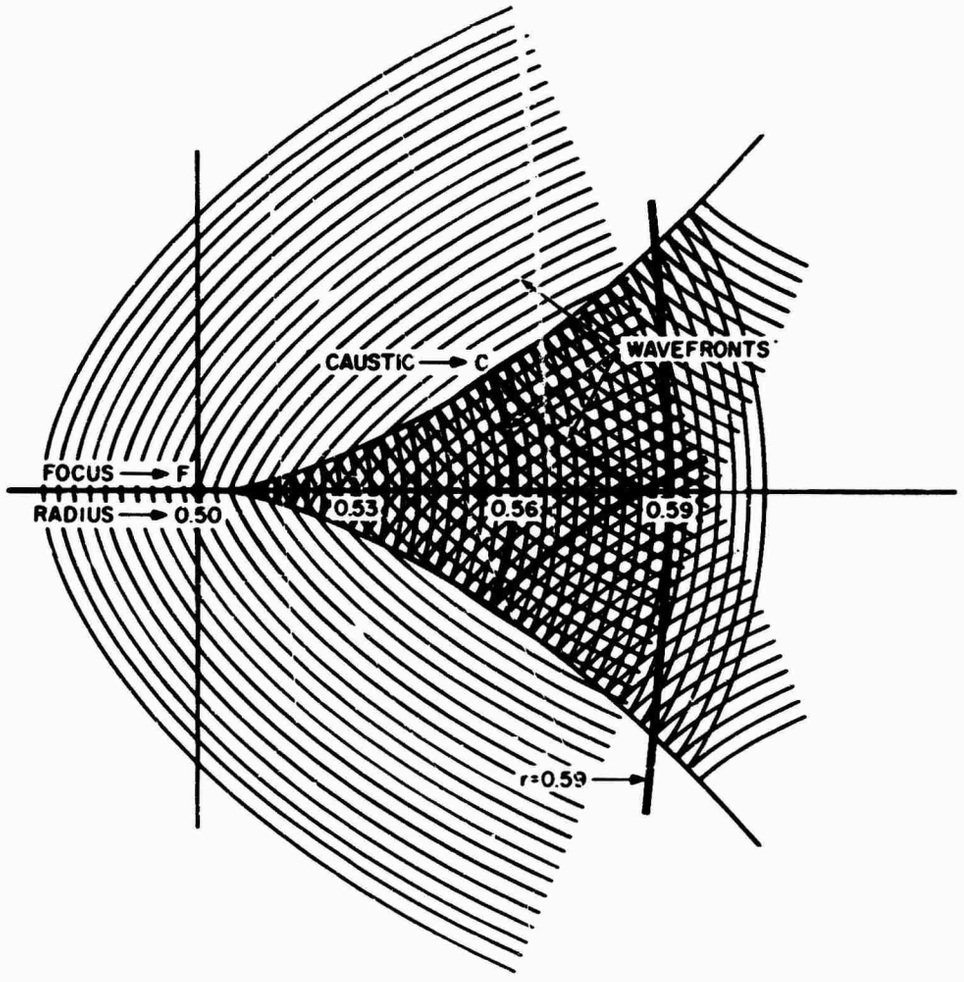

Figure 18. Wavefronts Constructed using Caustic Template

4.3 Rays and Wavefronts by Transmission

Up until now the sphere was considered as a receiver, illuminated by a distant point source. It was found that as many as three reflected rays, corresponding to three sets of wave fronts, could pass through a point Q in the focal region. Thus, an observer with one eye open at this point could see three brightly illuminated areas of the sphere similar to the flare spots when the sun shines on a polished auto body.

If now the observer and the source are interchanged, so that the observer is at a great distance, he will see the same areas of the sphere lighted up. These spots are in the direct line of sight of the images of the source which are located behind the mirror surface. This is illustrated by Figure 19 showing three images of a wood screw placed slightly toward the cylindrical mirror from its focus (that is, $r = 0.65$). There is extreme variation in the horizontal magnification of the three images. In fact, image B is about to stretch out and merge with image C. This is the same phenomenon that would be observed in the spherical mirror. The vertical magnification, however, is unity because the cylinder has no curvature along its axis.

Two other points are worth noting. The radial line r is imaged as a curve of two branches like that of a rectangular hyperbola. The upper left branch images the complete radius. The lower right branch cannot image any value of r less than

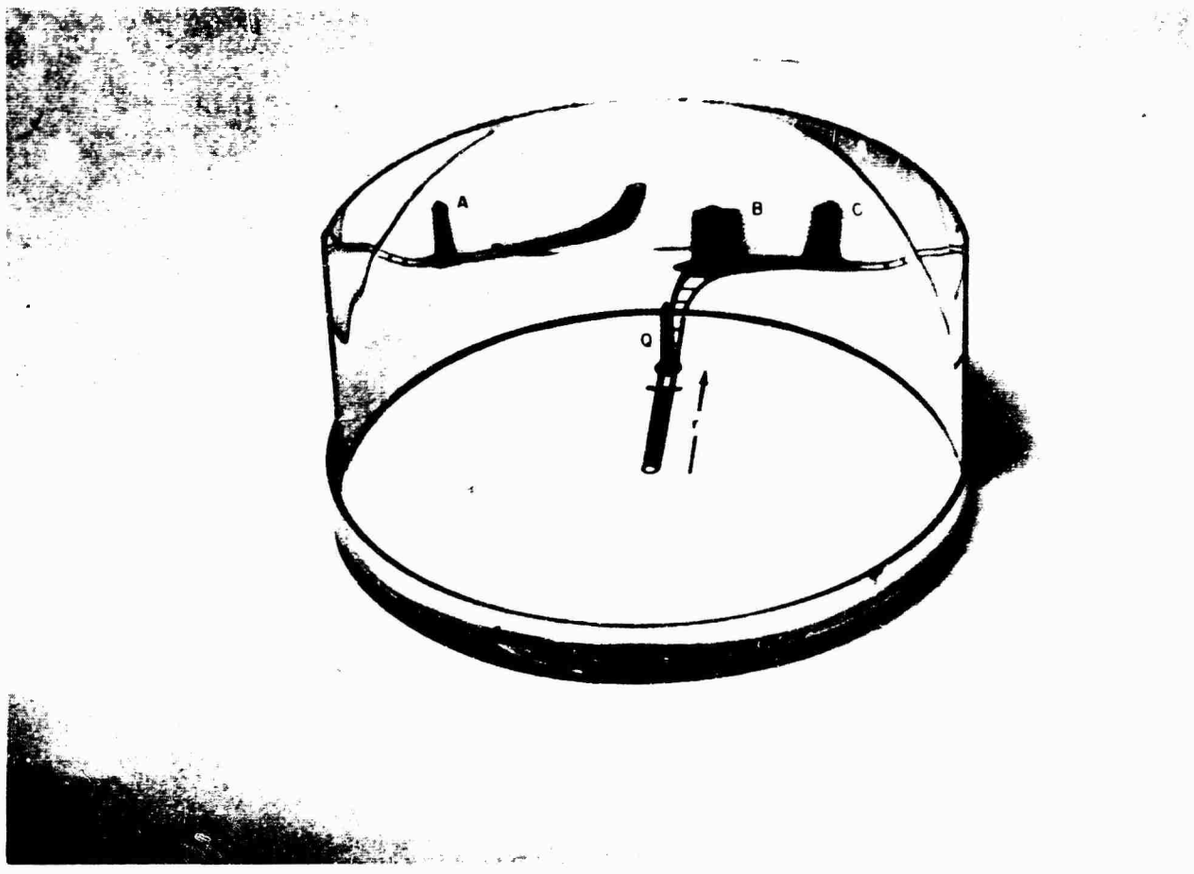

Figure 19. Images A, B, C of Screw Q in Cylindrical Reflector

0.5; and it repeats those values of r beyond the point on the caustic to which the radial line is tangent. Consequently, all three images lie on this two-branched curve.

The upper corners of this and the next figure show multiple reflections between opposite sides of the semi-cylinder, as well as distortion due to imperfection of the reflecting aluminum surface.

The second point is that the three images also lie on the image of the concentric circle of radius r, and continue to lie on it as the field point is moved on the constant radius. Figure 20 shows several of these concentric circles reflected in the cylindrical mirror. Note that the image of the circle with r = 0.5 is quite flat on the center while that of the 0.7 circle has a reverse curvature and depicts three images of the 7 in the foreground.

The wave front in the transmission case is a single valued function and is therefore less ambiguous than the receiving case. Thus, in Figure 21 the broken line QPA traces the optical path of a ray starting from the source Q and reflected from the cylindrical mirror at A in the direction PA. The angles of incidence and reflection are each α. If line is produced backward to Q' such that Q'P = QP, then the point Q' is a point on particular reflected wavefront with the same phase as at Q. Other points on wave front are obtained by allowing the point P to move around the circle, while on Q' traces the corresponding wave front. Naturally, the ray direction Q'P pendicular to the wave front at Q'.

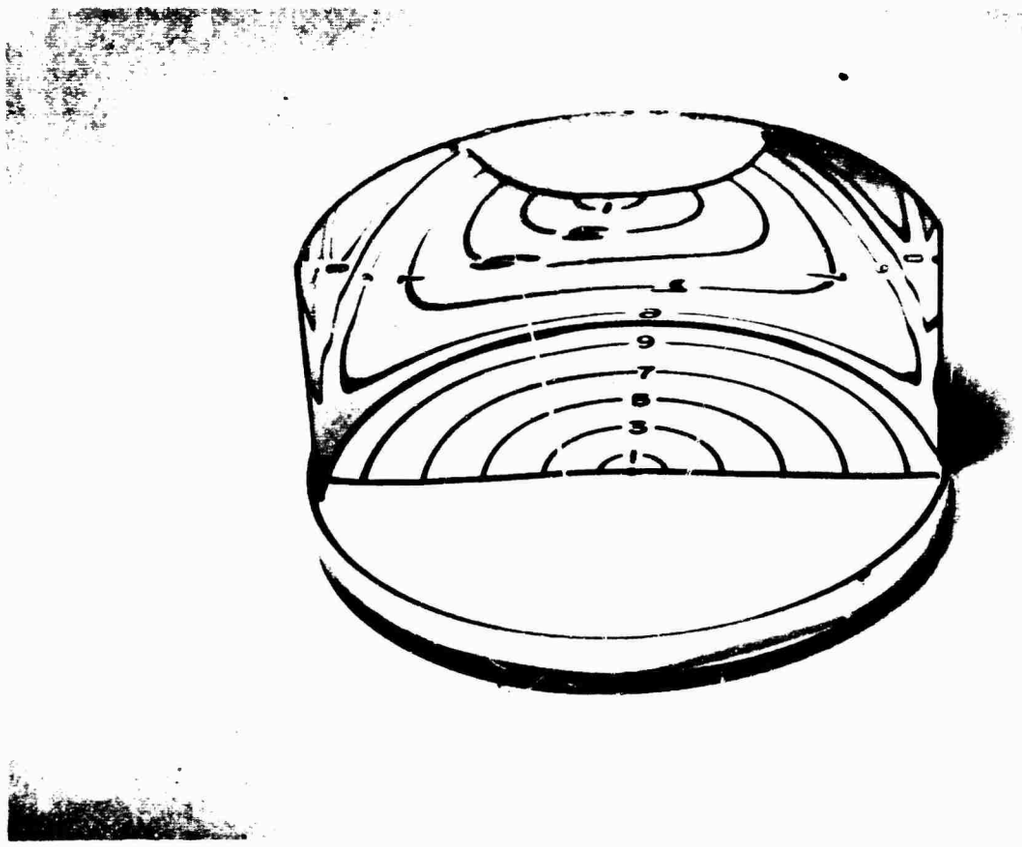

Figure 20. Reflections of Concentric Circles in Cylinder

There is an analogy between this wave front and the kinematics of gears. Consider two gears or discs of the same diameter in contact at point V and with centers O and O'. Let Q and Q' be points on the line of centers and equidistant from the point of contact V. Then as the gear with center O' rolls around the other, the point Q' moves to trace out the wave front of Figure 21. If Q were on the rim of the circle then Q' would trace out our old friend the epicycle (with equal sized gears, the particular one-cusp epicycle is a cardioid). However, with Q an interior point, the curve traced by Q' is a trochoid.[14] For equal sized gears this is the Limacon of Pascal discussed by Roberval in 1650.[15]

The wave fronts for r = 0.7 and 0.3 of Figure 21 are redrawn in Figure 22 with parallel tangents. The 0.7 curve has three tangent points at A, B, and C. When observed in a direction normal to these tangents the first Fresnel zone around each tangent point causes a flare spot. If the normal were perpendicular to the tangent at the point of inflection between points B and C, then we would have a double point. This occurs when the field point is on the caustic. The wave front for r = 0.3 shows but one tangent at D. This is characteristic of all field points for r < 0.5.

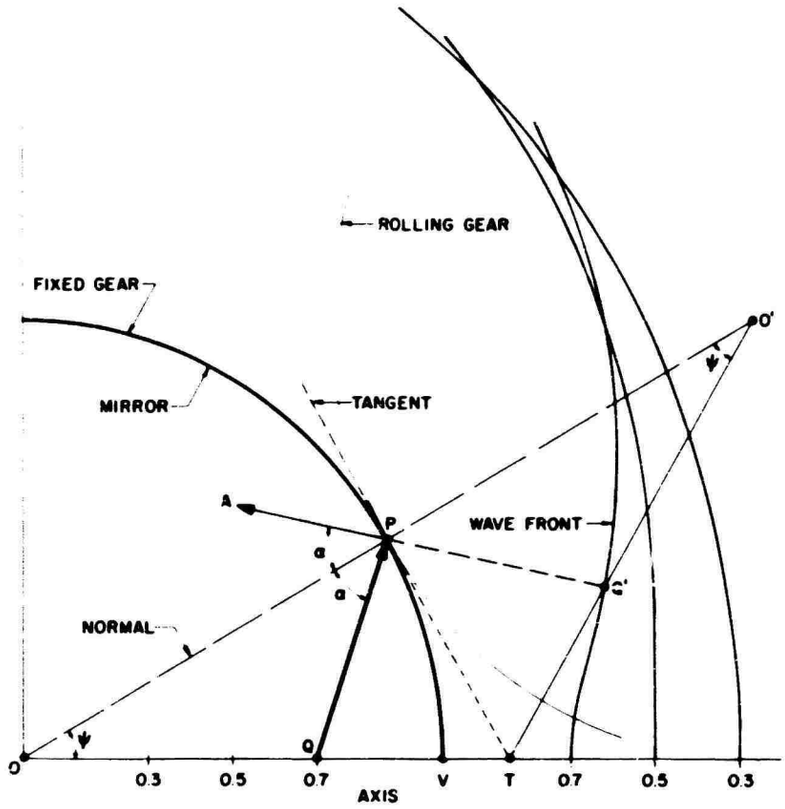

Figure 21. Reflected Wavefronts on Transmission from Sphere

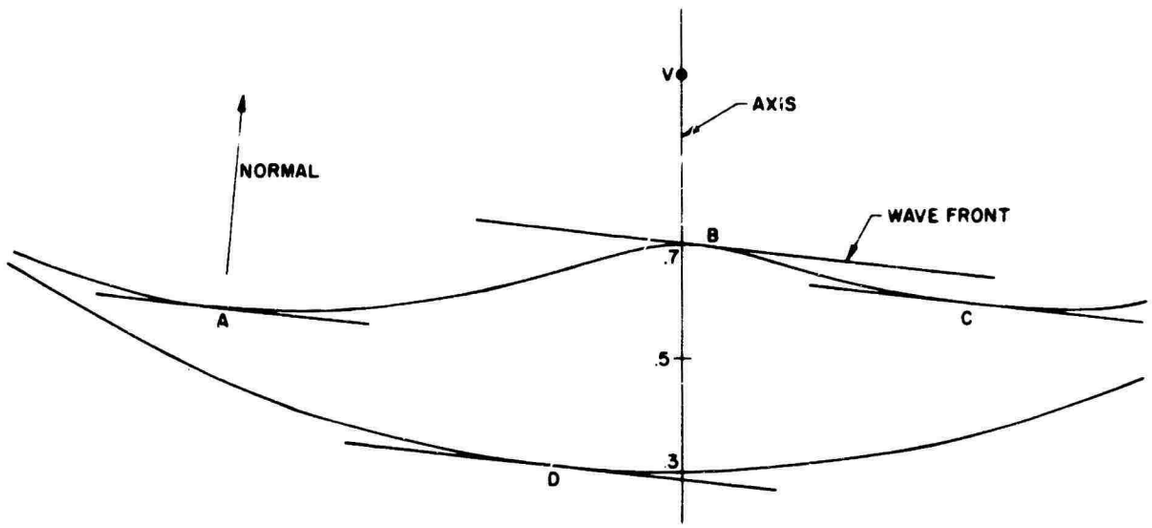

Figure 22. Three Parallel Tangents to Wavefront

5.0 PATH-LENGTH

In previous sections, optical rays and ray-tracing have been treated at some length. Of the properties of rays of interest in this study, perhaps the decisive one is optical path-length. It is the link between ray optics and wave theory. While it is derivable from geometric optics considerations alone, path-length enters into the expressions of wave theory as phase, and thus into the evaluation of that theory. Finally, stationary phase conditions may be explained partly in terms of geometric optics paths. It is for this reason that optical path-length is singled out for careful study and treatment.

5.1 Formulas for Path-length and Angles

The derivation of these formulas follows closely that of an unpublished memo by R. C. Spencer.

Figure 23 shows portions of concentric spherical surfaces of radii R and r_p. A ray AB parallel to the axis OV is reflected at B on the spherical reflector and is incident at P on the second surface. We have shown this as a feed surface, which it would be for a front-fed spherical reflector, but it could be a secondary reflector, as in a folded system.

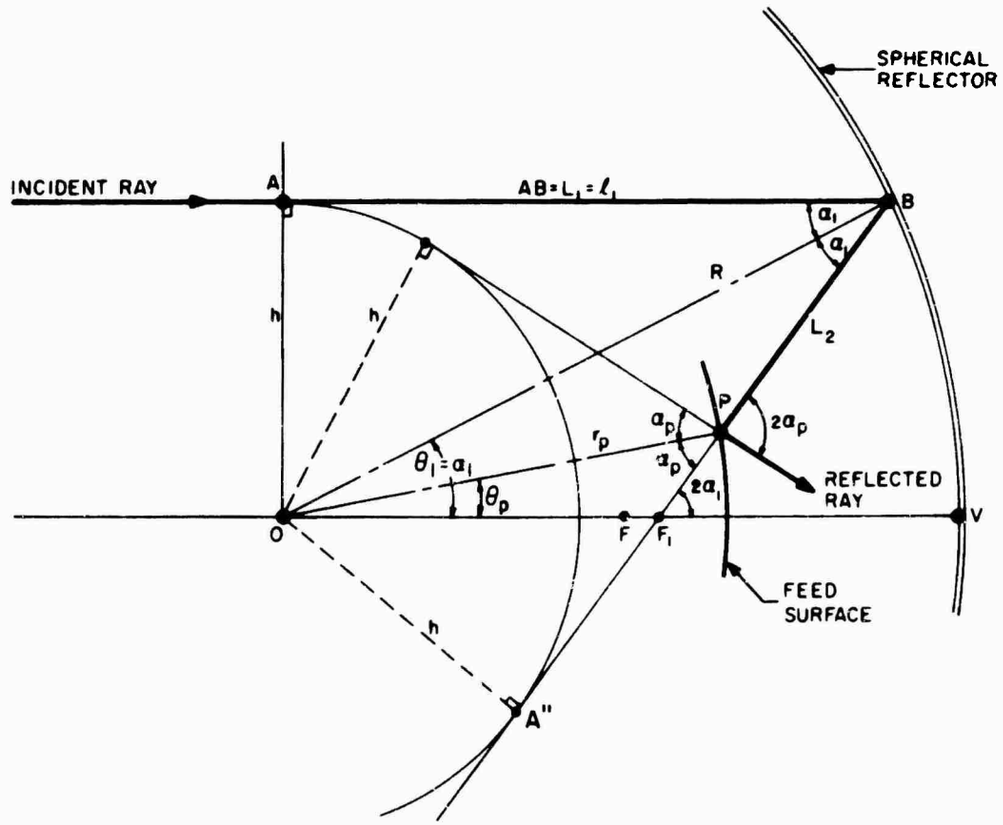

Figure 23. Reflection from Two Concentric Spheres

At B the law of geodesics*, $h = R \sin \alpha$, is obeyed, as it would be at P ($h = r_p \sin \alpha_p$), where α is the angle between ray direction and the normal, and h is the distance of closest approach of the ray to the center of curvature, 0.

(For a family of concentric surfaces we would have

$$h = r_1 \sin \alpha_1 = r_2 \sin \alpha_2 = r_3 \sin \alpha_3 = \ldots)$$

Since OV is parallel to AB, then

$$\theta = \alpha,$$

and

$$\measuredangle VF_1B = 2\alpha.$$

From triangle F_1PO,

$$\theta_p = 2\alpha_1 - \alpha_p = 2 \sin^{-1}\left(\frac{h}{R}\right) - \sin^{-1}\left(\frac{h}{r_p}\right) \tag{37a}$$

(For a family of N concentric surfaces,

$$\theta_n = 2\alpha_1 - 2\alpha_2 + 2\alpha_3 - \ldots + (-1)^{n+1}\alpha_n$$

$$= 2 \sin^{-1}\frac{h}{r_1} - 2 \sin^{-1}\frac{h}{r_2} + \ldots + (-1)^{n+1}\sin^{-1}\left(\frac{h}{r_n}\right)$$

The optical path-length from the reference line OA to B is AB. Then

$$L_1 = AB = \ell_1 = R \cos \alpha = (R^2 - h^2)^{1/2} \tag{38a}$$

The optical path-length L from A to P is AB + BP.

But

$$L = AB + BP = AB + BA'' - PA'' = 2AB - PA''$$

since

$$BA'' = AB.$$

*At any point along a geodesic in an axially symmetric system the following law holds $\mu r \sin \alpha = h$, a constant, where μ is the relative index of refraction, α the angle the ray makes with the meridian through the point and r is the shortest distance from the point to the axis. The law is equally useful for geodesics over surfaces of revolution anf for optical systems. For reflectors, $\mu = 1$.

If we denote PA'' as ℓ_p,

$$\ell_p = (r_p^2 - h^2)^{1/2}$$

and

$$L = 2\ell_1 - \ell_p \tag{39}$$

(For a family of concentric surfaces, if L is the path-length to a point on the nth surface,

$$L = 2\ell_1 - 2\ell_2 + 2\ell_3 - + \ldots + (-1)^{n+1}\ell_n$$

where

$$\ell_n = (r_n^2 - h^2)^{1/2} \tag{38b}$$

The usefulness of knowing the path-length to and the angular coordinate of a point on a surface, given the radius to that point and the height of the incoming ray, is immediately evident. However, on the graphs of L and θ plotted against h, the caustic surface occurs for stationary values, i.e.

$$\frac{dL}{dh} = 0; \quad \frac{d\theta}{dh} = 0$$

Hence it is also useful to know these derivatives as well.

Noting that

$$\alpha = \sin^{-1}\frac{h}{r} = \frac{h}{r} + \frac{1}{2\cdot 3}\frac{h^3}{r^3} + \frac{1\cdot 3}{2\cdot 4\cdot 5}\frac{h^5}{r^5} + \ldots$$

then

$$\theta_p = h\left(\frac{2}{R} - \frac{1}{r_p}\right) + \frac{h^3}{2\cdot 3}\left(\frac{2}{R^3} - \frac{1}{r_p^3}\right) + \ldots$$

Expanding the equation for L, one gets

$$L = \left(2R - r_p\right) - \frac{h^2}{2}\left(\frac{2}{R} - \frac{1}{r_p}\right) - \frac{h^4}{8}\left(\frac{2}{R^3} - \frac{1}{r_p^3}\right) - \ldots \tag{40}$$

and on differentiating, one finds

$$\frac{dL}{dh} = -h\frac{d\theta}{dh} \tag{41}$$

whence

$$\frac{dL}{d\theta} = -h$$

(This remarkably simple equation can also be derived from a differential triangle.)

Now

$$L = 2\ell_1 - \ell_p = 2(R^2 - h^2)^{1/2} - (r_p^2 - h^2)^{1/2}$$

Hence

$$\frac{dL}{dh} = -h\left(\frac{2}{\ell_1} - \frac{1}{\ell_p}\right) \tag{42}$$

and

$$\frac{d\theta}{dh} = \frac{2}{\ell_1} - \frac{1}{\ell_p} \tag{43}$$

Computationally, it proves useful to normalize all lengths with respect to R. Thus the computations done for the single reflector feed surface case were made using the formulas

$$L = 2\ell_1 - \ell_p \tag{39}$$

$$\theta = 2\sin^{-1} h - \sin^{-1}\frac{h}{r_p} \tag{37b}$$

$$\frac{d\theta}{dh} = \frac{2}{\ell_1} - \frac{1}{\ell_p} \tag{43}$$

$$\frac{dL}{dh} = -h\frac{d\theta}{dh} \tag{41}$$

where

$$\ell_1 = (1 - h^2)^{1/2} \tag{38c}$$

$$\ell_p = (r_p^2 - h^2)^{1/2} \tag{38d}$$

Taking the results of these computations, we have graphed L, θ, dL/dh and $d\theta$/dh as functions of h. Let us examine the plot of L against h (Figure 24). It is immediately evident that L is an even function of h i.e., has even symmetry about h = 0. (One can represent the half-plane $\phi - \pi$ by negative values of h.) Thus ray path-lengths are the same in each half plane, and there may be as many as four rays of

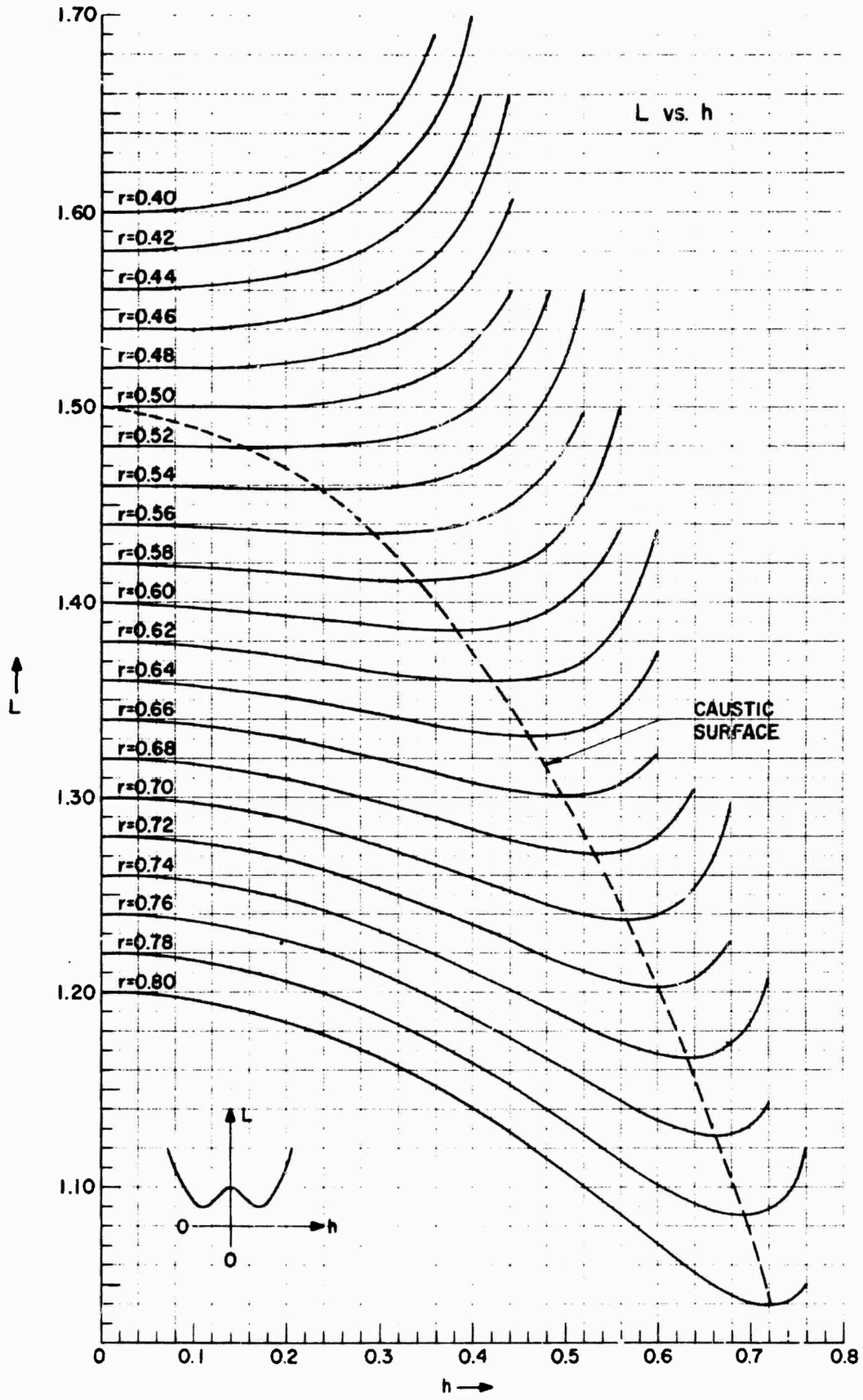

Figure 24. Path-Length versus h

the same path-length. Note that the slope of the L vs. h curves is always zero at h = 0, the axial caustic, but has other stationary values only for $r_p > 0.50$. This is because the caustic surface does not exist for $r_p < 0.50$. The locus of the caustic is noted on the graph. The other point worth noting is the increasing range of variation of L within the caustic surface as r_p increases. This greater variation of path-length implies wider ranges of phase. The curves of dL/dh vs. h (Figure 25) are noteworthy, principally in that the zeroes lie on the caustic surface and the manner in which the curves "take off" after crossing the zero line, indicating a rapidly increasing increase in path-length outside the caustic. These curves have odd symmetry about h = 0.

One of the more interesting graphs is the set of curves of θ vs h (Figure 26). Now these curves have odd symmetry, and what this means is that if we choose a value of r_p, and θ_p, i.e. a fixed point, there are three values of h, i.e., three rays which pass through some field points (r_p, θ_p). This verifies our earlier observation, and provides an easy way of locating the three incident rays. As with the curves of L vs h, the stationary points are the locus of the caustic surface on the graph. Note that there are no stationary values for $r_p < 0.50$. The curves of $d\theta/dh$ vs h are shown in Figure 27. As expected, they show even symmetry. Again, the zeroes of $d\theta/dh$ lie on the caustic surface. As a check one may note that $h\, d\theta/dh = -dL/dh$.

From the computed data, curves for L vs θ_p were plotted (Figure 28). Almost all the properties seen in the other curves are to be found in these "fish tails". For example, the cusps, or points on the tails of the "fish tail", mark the locus of the caustic surface. A line of constant θ_p has up to three intersections with any plotted curve for constant r_p, denoting the three rays through a field point previously discussed. A line of constant L has as many as four intersections with plotted curves. The shrinking of the tail of the "fish tail" as r_p decreases, is, of course due to the shape of the caustic surface, tapering to a cusp at the paraxial focus.

If one considers a particular feed surface (curve for constant r_p), it is interesting to trace the change in path-length as θ_p is varied. There are three branches to the "fish tail"; the semi-circular sector between the cusps and the two long arms. One can identify the associated rays. Let us use $r_p = 0.6$ as an example. For θ_p outside the cusps, say $\theta_p = 10^o$ there is a point on one arm only. This must be due to the ray that exists outside the caustic, i.e., the ray from the "other" half plane (that not containing the field point). As θ_p approaches the axis ($\theta_p = 0$), the two "arms" intersect, on the axis. This can occur only for rays at equal height. So the other "arm" must represent the outermost ray on the same side of the axis as the field point. The remaining segment, the semi-circular sector is the locus of the "inner" ray. Note that the two rays on the same side approach one another in path-length before vanishing on the caustic surface as the field point approaches the caustic. It is interesting that the "inner" ray undergoes comparatively little change in path-length over the focal region, while the other two rays change considerably, and in opposite directions.

One should not be deceived by the small changes in path-length normalized with respect to the radius of curvature of the spherical reflector. Typical reflectors may have radii of curvature of 150 to 300 wavelengths, so that a change of 0.01 on the graphs may be 1.5 to 3 wavelengths, or 500^o to 1000^o of phase. If one

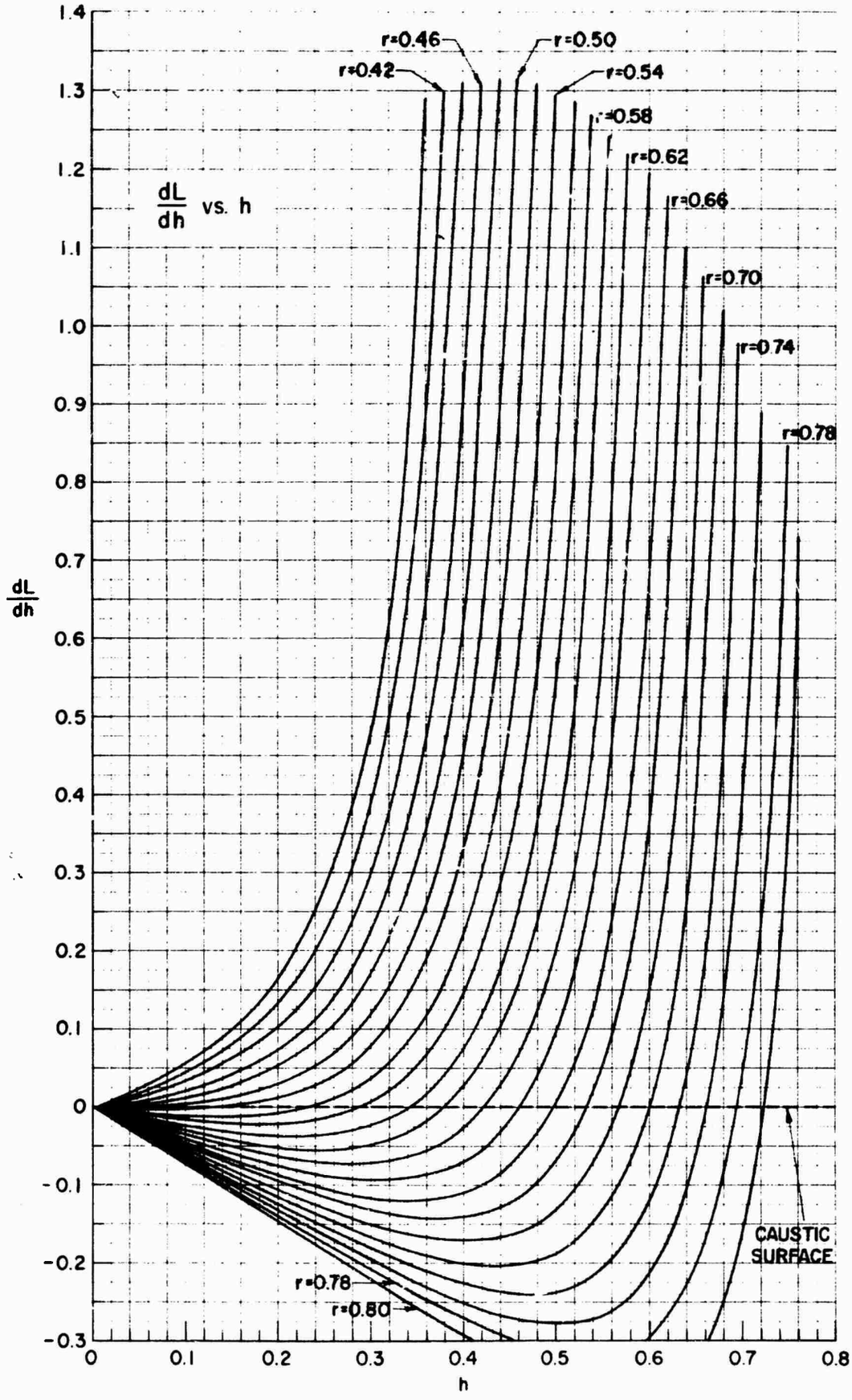

Figure 25. Derivative of Path-Length versus h

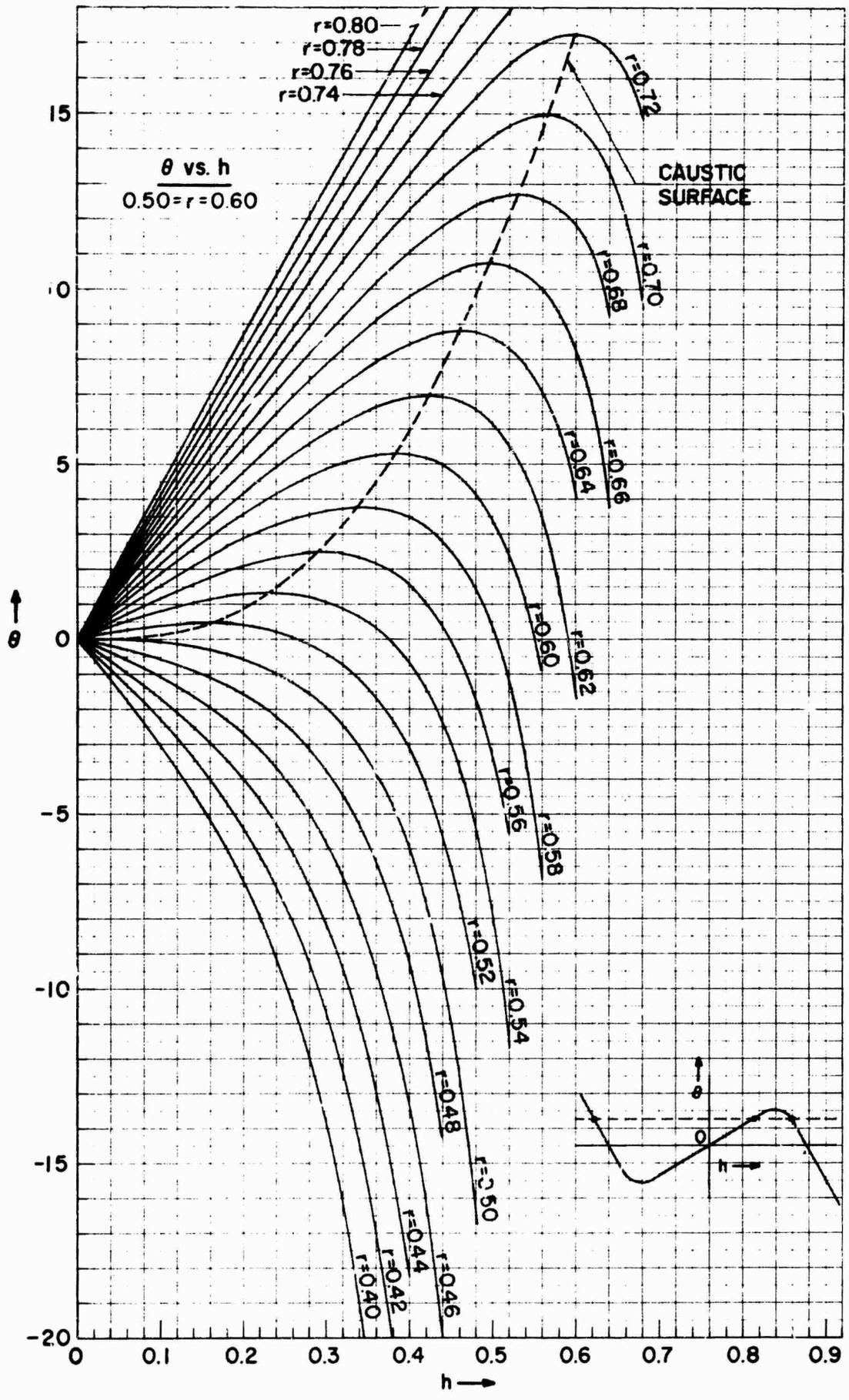

Figure 26. θ versus h

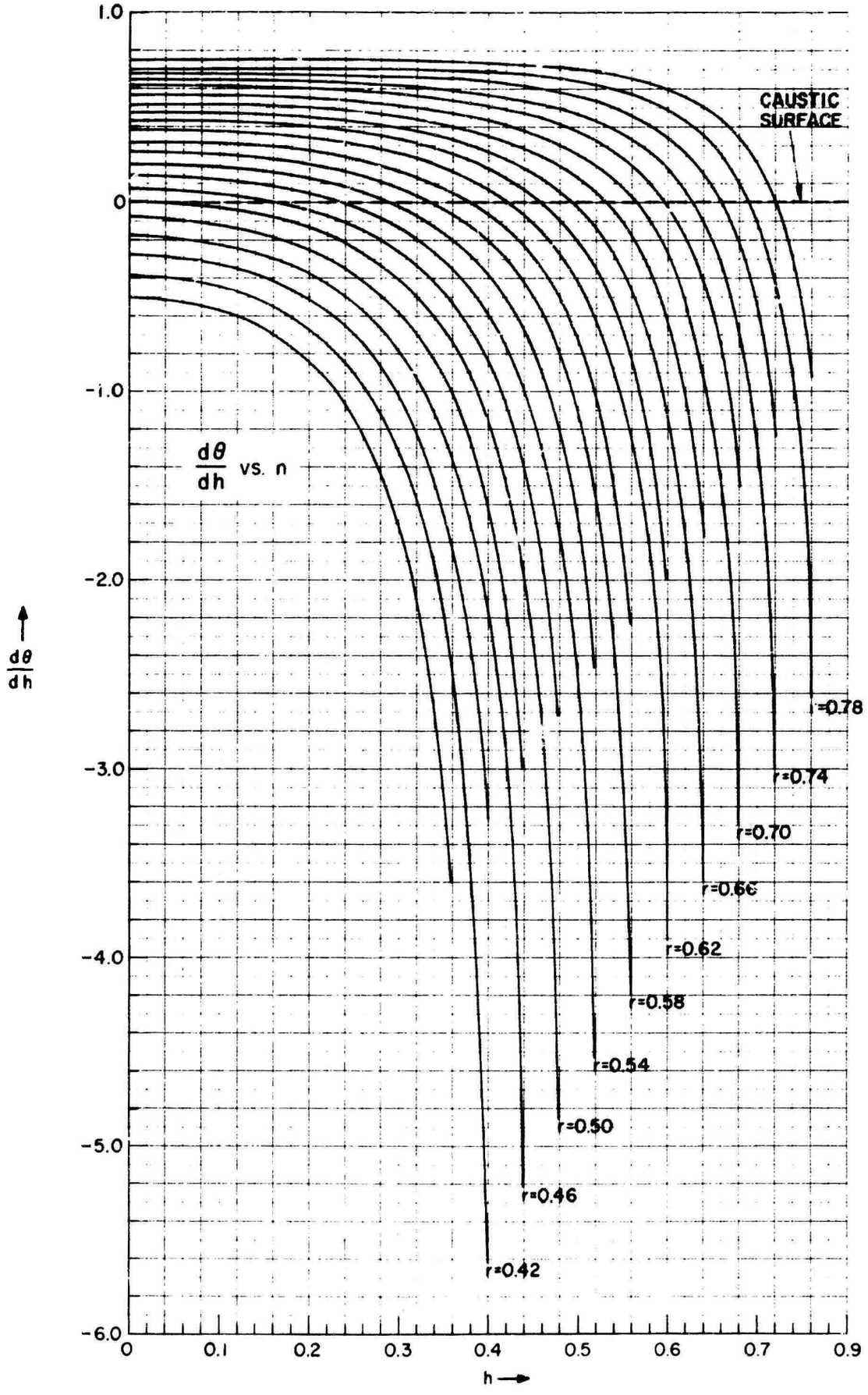

Figure 27. Derivatives of θ versus h

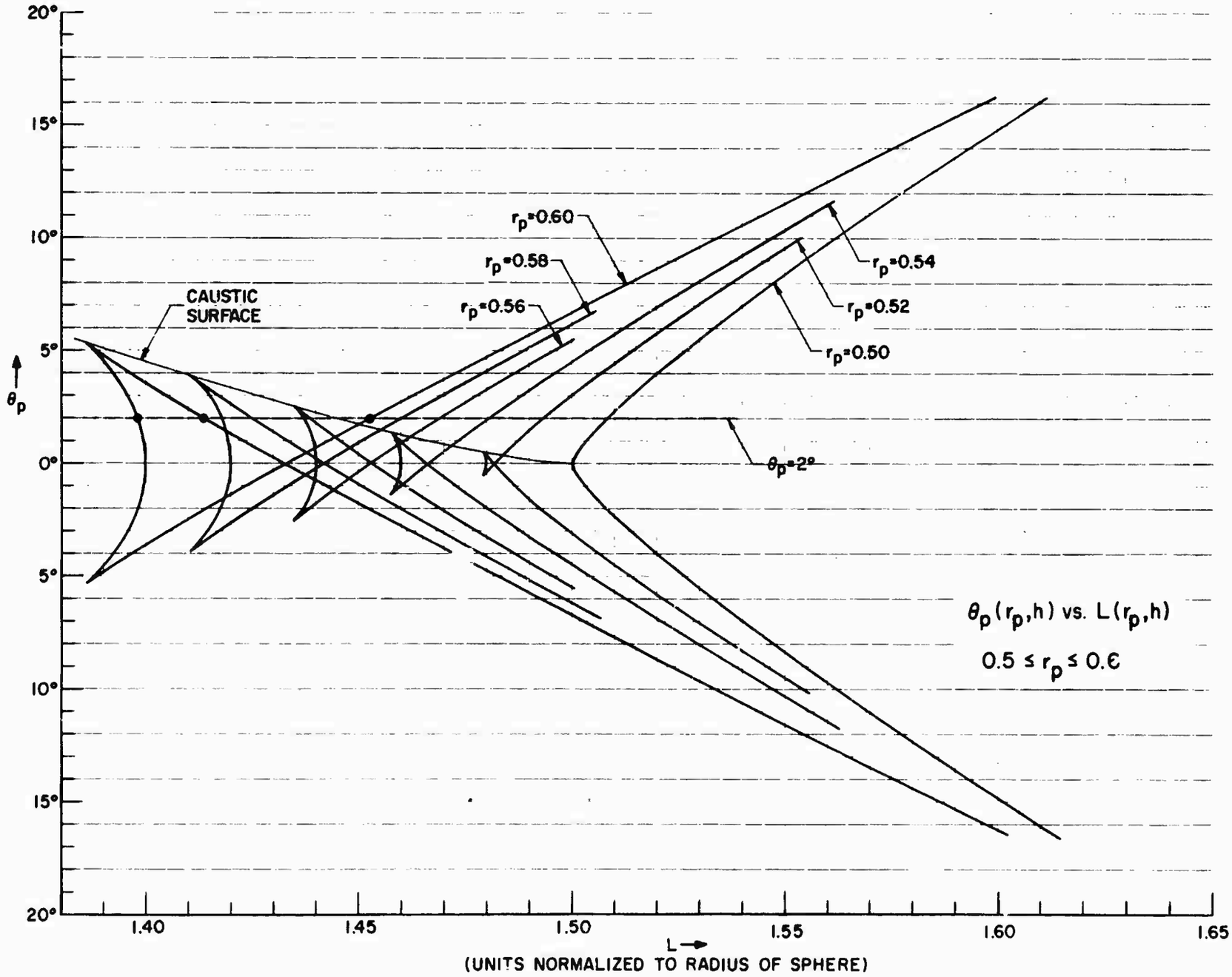

Figure 28. θ versus Path-Length

considers 90^{o} of phase change to be quite important, this means that changes in the fourth significant figure of normalized path-length are worthy of note. This means that the optical path-length of even the slowly varying "inner" ray changes very significantly in the regions of interest, while the other rays are much worse.

Figure 19 shows a particularly apt demonstration of the existence of three regions of stationary phase. It is the inverse of our case, as the small screw imaged three times in the cylindrical mirror is in the focal region, and is viewed from a distance.

5.2 Path-Length and Stationary Phase

The relationship between path-length in geometric optics and the method of stationary phase should be emphasized. It is planned to use this method in evaluating certain integrals that have arisen in viewing this problem from electromagnetic wave diffraction. Path-length and electromagnetic phase are equivalent. Specular reflection results from stationary phase taken to the limit of short wavelengths. While the method of stationary phase is often considered to have limitations mathematically speaking, it is very strong physically because it is founded on physical and geometric optics. The conditions on our variables in stationary phase turn out to be conditions on path-length and path-length derivatives. We impose the conditions $dL/d\phi = 0$, $dL/d\theta = 0$. And these give rise to the relationships,

$$\phi - \phi_p = \begin{cases} 0 \\ \pi \end{cases}$$

and

$$\frac{\sin \theta}{r_p} = \frac{\sin (\theta \pm \theta_p)}{L_2} \tag{44}$$

The meaning of these two relationships is readily arrived at from our earlier work. The first was implied in Section 2, where it was shown that all rays remain in their plane of incidence. The second is simply the sign law for triangle OPB of Figure 23. This ultimately is our justification for the approach to the problem through geometric optics. It has a bearing on the answers we are obtaining in our further study.

This further study emphasizes the aforementioned approach to the problem through stationary phase and experimental measurements. In the former, it is intended to evaluate the field of points in the focal region. This evaluation will take account both of polarization and of the multiplicity of contributions. The experimental effort will be mainly directed towards a corrected transverse feed with some scanning possibilities. There will be a limited amount of work directed at verification of the theoretical study.

REFERENCES

1. Boivin, Albéric, Théorie et Calcul des Figures de Diffraction de Révolution, Université Laval, Quebec, Canada (1960).

2. B. Richards, E. Wolf, "Electromagnetic Diffraction in Optical Systems II. Structure of the Image Field in an Aplanatic System", Proceedings of the Royal Society, A, Vol. 253, pp. 358-379, February 1959.

3. F. A. Jenkins and Harvey E. White, "Fundamentals of Optics", Second Edition, McGraw-Hill Book Company, Inc. (1950) pages 89 to 92 and 123 to 132. This gives a brief, plausible explanation of spherical aberration and astigmatism.

4. R. C. Spencer, C. J. Sletten and J. E. Walsh, "Correction of Spherical Aberration by a Phased Line Source", Proceedings of the National Electronics Conference (Vol. 5) Chicago, (1950).

5. Encyclopedia Brittanica, CURVES, SPECIAL-THE NEPHROID. The "Nephroid" is so-named because of its resemblance to the kidney.

6. Robert C. Yates, "A Handbook on Curves and Their Properties", J. W. Edwards - Ann Arbor - 1947. This is a remarkable reference book with curves, formulas and definitions. It is well indexed. Topics pertinent to our problems are: cardioid, caustic, cycloid, envelopes, epi-cycloid, evolute, Nephroid, parallel curves, roulettes, also the intrinsic equations.

7. C. Zwikker, "Advanced Plane Geometry", North Holland Publishing Company, Amsterdam, 1950. Also published in a paperback edition by Dover Publications, Inc., New York, N. Y. Zwikker discusses many types of curves using complex number notation. The analysis of section 3.2, much of which was developed by R. C. Spencer in an unpublished memo prior to the publishing of Zwikker's book, is in general agreement with Zwikker.

8. Yates, loc. cit., pages 125, 126.

9. Yates, loc. cit., pages 125, 126.

10. Yates, loc. cit., page 89, Figure 83.

11. Zwikker, loc. cit., pages 144, 183.

12. Yates, loc. cit., pages 155-159.

13. Yates, loc. cit., pages 175-185, 135.

14. Yates, loc. cit., page 233.

15. Yates, loc. cit., pages 148-151.